Georg Kügerl, BSc

Interaction between PLZT ceramics and Copper electrodes

MASTER'S THESIS

to achieve the university degree of

Diplom-Ingenieur

Master's degree programme: Technical Chemistry

submitted to

Graz University of Technology

Supervisor

Ao.Univ.-Prof. Dr. Klaus Reichmann

Institute for Chemical Technology of Materials

in corporation with the EPCOS OHG, A TDK Group Company

Graz, April 2016

AFFIDAVIT

I declare that I have authored this thesis independently, that I have not used other than the declared sources/resources, and that I have explicitly indicated all material which has been quoted either literally or by content from the sources used. The text document uploaded to TUGRAZonline is identical to the present master‘s thesis.

Date	Signature

Abstract

The increasing price of noble metals during last decades was responsible for copper becoming an interesting electrode material in Lead based electro-ceramic components. Within this context, the basic behavior of copper oxide as a dopant and copper as electrode material in Lead Lanthanum Zirconate Titanate (PLZT) have been in focus of this thesis. Special attention was paid to the preparation of representative samples which can only be produced in a well-defined process. Therefore PLZT was modified by adding varying amounts of copper oxide and processed under different conditions which were influencing the redox behavior. Gravimetrical control yielded information about the state of oxidation after the process steps. XRD measurements undergirded the results of the gravimetrical determination and identified copper/copper oxide precipitates in the material. The grain structure was determined by scanning electron microscopy and the amount as well as the shape of copper oxide precipitates in the material were studied by optical microscopy. The influence of copper oxide on the electrical properties was investigated, the limit of solubility of the dopant was determined and its impact on the sintering process was clarified.

Kurzfassung

In den letzten Jahrzehnten führte der Preisanstieg von Edelmetallen zu einem erhöhten Interesse an Kupfer als Elektrodenmaterial in elektrokeramischen Bauteilen auf Bleibasis. Dadurch wurde das Verhalten von Kupferoxid als Dotierstoff und Kupfer als Elektrodenmaterial in Blei Lanthan Zirkontitanat (PLZT) zum Thema dieser Arbeit. Die Herstellung von repräsentativen Proben in einem klar definierten Prozess stellte sich als entscheidender Schritt heraus. PLZT Umsatzpulver wurde mit unterschiedlichen Kupferoxidmengen versetzt und unter verschiedenen Bedingungen thermisch prozessiert, was sich unterschiedlich auf das Redoxverhalten auswirkte. Die gravimetrische Kontrolle der Proben lieferte Information über den Oxidationszustand nach dem jeweiligen Prozessschritt. Mit Hilfe von Röntgenbeugungsexperimenten wurde das Einlagerungsverhalten in Bezug auf die Veränderung der kristallografischen Einheitszelle bestimmt. Des Weiteren konnten Informationen über das Redoxverhalten von Kupferoxid während der Prozessschritte durch charakteristische Reflexe der jeweiligen Kupfer- bzw. Kupferoxid-Sekundärphasen erhalten werden. Die daraus resultierenden dielektrischen Eigenschaften wurden erfasst. Mit Rasterelektronenmikroskopie wurde der Einfluss auf das Gefüge überprüft und die Anzahl beziehungsweise die Form der Kupferoxid Ausscheidungen wurden mit dem Lichtmikroskop erfasst. Mit diesen Methoden konnte die Löslichkeitsgrenze von Kupferoxid in der Keramik bestimmt werden, der Einfluss auf den Sinterprozess wurde deutlich gemacht und die elektrischen Eigenschaften wurden geprüft.

Danksagung

Ein besonderer Dank gilt Herrn Ao.Univ.-Prof. Dr. Klaus Reichmann für die ausgezeichnete Betreuung.

Ich möchte mich bei der Firma EPCOS OHG, Teil der EPC-TDK Gruppe für die Bereitstellung der Rohstoffe, die Benützung sämtlicher Geräte und Arbeitsutensilien sowie die finanzielle Zuwendung bedanken.

Ein großes Dankeschön gebührt Herrn Dr. Manfred Schweinzger, dem Leiter der Abteilung Corporate Materials Research and Development für die Ermöglichung und Durchsicht dieser Masterarbeit.

Ich möchte mich außerdem beim gesamten Team der Corporate Materials Research and Development Abteilung für die gute Zusammenarbeit und die Unterstützung während der Diplomarbeit bedanken. Ein großes Dankeschön geht im Besonderen an folgende Personen:

Herrn Dr. Michael Schossmann für seine Ratschläge um die Themen Thermische Prozesse, Physikalische Vorgänge im Gitter und Elektrische Charakterisierungen.

Herrn Dr. Denis Orosel für seine Mithilfe durch Erfahrung und Wissen bei der Auswertung der Röntgen Diffraktrogramme.

Frau Dr. Kerstin Schmoltner und Frau Dr. Theresa Kainz danke ich recht herzlich für Ratschläge und Tipps aller Art.

Herrn Peter Horn für die Anweisungen und Unterstützung bei der Probenvorbereitung und Bildaufnahme bei der Optischen und Raster Elektronen Mikroskopie.

Herrn Dr. Bernd Döllgast und Herrn Dr. Alexander Glazunow für ihre unverzichtliche Hilfe bezüglich der Thermischen Prozesse.

Herrn Dipl. Ing. Peter Windisch, Leiter des Analytiklabors, für die Benützung der Analysengeräte.

Frau Heidi Cebular, Frau Claudia Lenzbaurer, Frau Margarethe Pölzl und Herrn Thomas Resch für die großartige Unterstützung.

Table of content

1 Introduction

Due to the increasing price of noble metals, used as electrodes of electro-ceramic components, the research and development aim was set on cheaper alternatives.

The search for methods for equilibrium processing of Nickel and Iron as base metal electrodes in $BaTiO_3$ was begun in the 1960s [1, 2]. The success of this method is strongly dependent on the thermodynamic equilibrium adjusted between the oxide material and the base metals. The equilibrium can be driven in a certain direction by the adjustment of the oxygen partial pressure either by control of H_2/H_2O or CO/CO_2 ratio during processing. Within this background multilayered electro-ceramic components containing inexpensive nickel- electrodes have been produced [3].

Unfortunately nickel as electrode material does not work in lead based ceramics. In the Richardson-Ellingham plot the equilibrium line between a metal and its oxide is monitored over the temperature with respect to the oxygen partial pressure. The stability function of Pb/PbO lies at higher oxygen partial pressures than the one of Ni/NiO. Lead is nobler than Nickel, therefore PbO gets reduced to Pb at an oxygen partial pressure, where Ni is oxidized to NiO before the oxygen partial pressure is on a level where Ni remains reduced.

Some other solution needed to be found. One of the most promising alternative was copper, which is qualified through high electrical conductance, a higher electronegativity – a more noble character and a cheaper price than noble metals, which were used before.

Widely known new inventions open a can of worms. Copper has been used as a sintering aid in Lead Zirconate Titanate (PZT) before. Investigations about the influence on piezoelectric properties, the impact on the densification and the microstructural development have already been performed [4]. The fine tuning of the process on industrial scale was achieved by EPCOS, now member of the TDK group, and the industrial production of e.g. actuators has been operated for years. However process dependent problems leaded to a higher priority of interest in the chemical and physical processes in the material. Therefore this work will mainly focus on the influence of the processing conditions on the incorporation or segregation of copper compounds in PLZT.

Following sections of the introduction will provide the background for understanding the topic. PLZT ceramics, defects in the material, the key issues of copper and typical

electrical properties will be described. In the experimental part the sample preparation and the characterization methods are outlined. The last chapter, results and discussion will reflect the gained information and deal with the interpretation of those.

1.1 Lead Zirconate – Lead Titanate and its Structures

1.1.1 General Aspects

1.1.1.1 Perovskite Structure

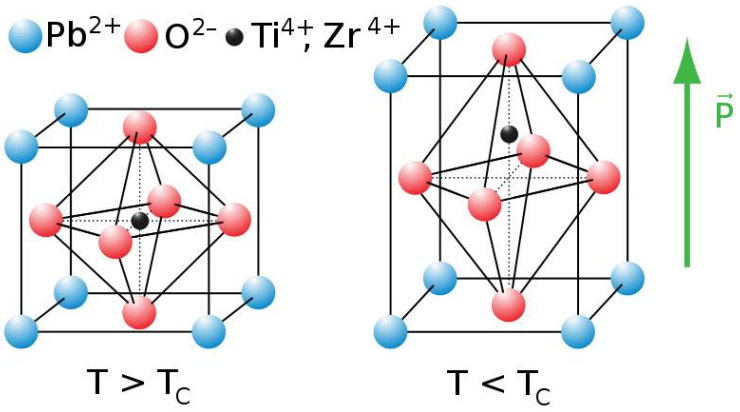

Figure 1 – PZT type perovskite structure below (with spontaneous polarization) and above the critical temperature (Curie temperature) [5]

The name perovskite is derived from the mineral calcium titanate, $CaTiO_3$. It was discovered in 1839 in the Ural Mountains by Gustav Rose and named after the mineralogist Lev Perovski. [6] The structure (Figure 1) itself was discovered and described by Victor Goldschmidt in 1926. [7] The general formula ABO_3 contains A (radius > 1Å; coordination number: 12) and B site occupying species (radius < 1Å; coordination number: 6) as common metal atoms. It can be described as face centered cubic cell (fcc) with the A atoms in the corners, the oxygen atoms occupy the centers of the surface- squares and additionally the B atom fills up the center. Therefore 8 x 1/8 = 1 A- atom, 1 x 1 = 1 B- atom and 6 x 1/2 = 3 O- atoms can be found in this cubic cell.

Many different materials, mostly oxides as well as halides, occurring naturally but also synthesized exhibit this structure.

1.1.1.2 Solubility

Similar to liquid/solid systems (e.g. salt in water), there is a limited solubility of components in solid/solid systems. In some of the systems isovalant exchange occurs. This means infinite solubility of two components.

It generates the opportunity to create PZT of all different compositions by mixing lead titanate and zirconium titanate. (Figure 2)

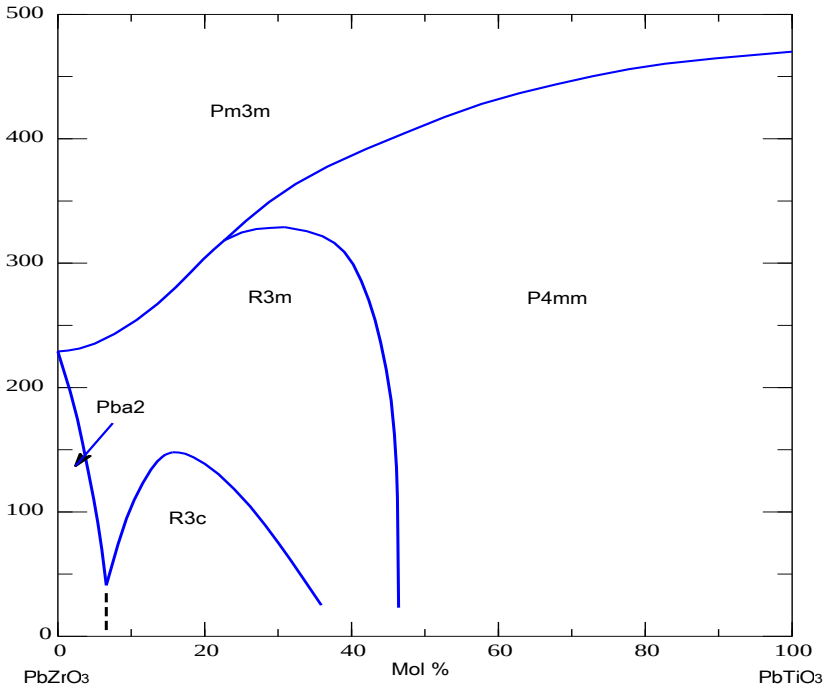

Figure 2 – System $PbZrO_3$-$PbTiO_3$. Phase transitions in lead zirconate-titanate solid solutions. Pm3m = cubic solid solution $Pb(Zr,Ti)O_3$; P4mm = tetragonal solid solution $Pb(Zr,Ti)O_3$; R3m and R3c = rhombohedral solid solutions $Pb(Zr,Ti)O_3$; Pba2 = orthorhombic solid solution $Pb(Zr,Ti)O_3$, Temperature [°C] [8]

As revealed in Figure 2 different symmetries depending on the composition of the material and the temperature are present. Throughout different phase transitions and other changes of dimensions of the lattice a lot of technically useful properties can be figured out. Observed properties are e.g. magnetoresistance, ferroelectricity, superconductivity, charge ordering, spin dependent transport, high thermopower and the interplay of structural, magnetic and transport properties [9]. All those properties can be achieved through, processing, doping and design according to the requirements in a certain device.

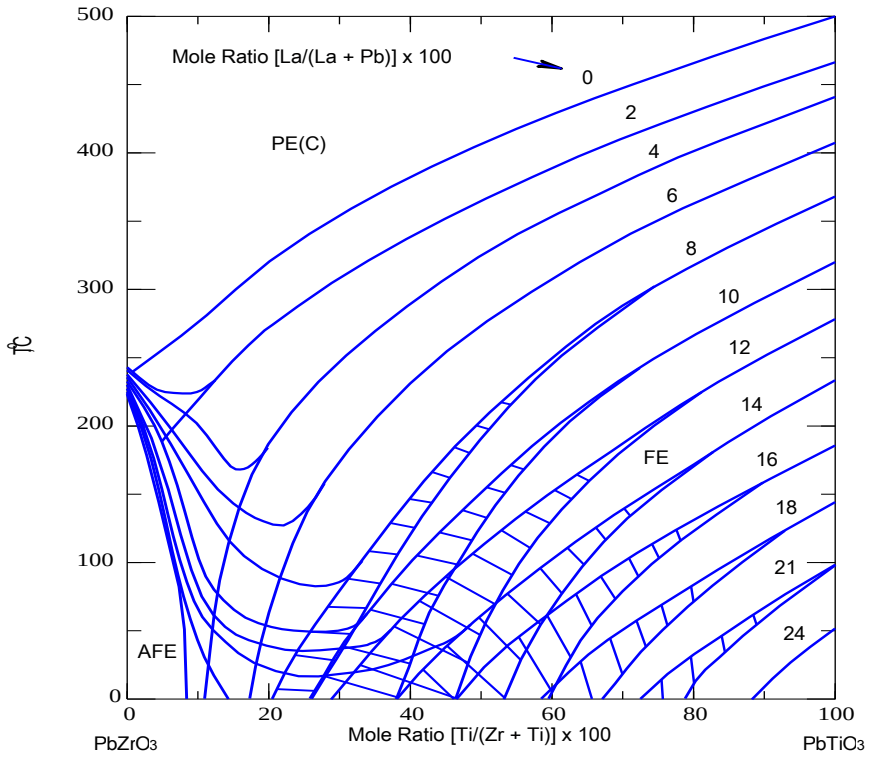

Figure 3 - System PbO-ZrO_2-TiO_2-La_2O_3 phase transitions as a function of temperature. FE(R), FE(Tet), AFE, PE(C), refer to rhombohedral and tetragonal ferroelectric, antiferroelectric, and nonferroelectric (paraelectric) cubic phases, respectively. [10]

Figure 3 monitors information about the system with 7 mol% Lanthanum, which is used in this thesis. With a Zr content of 86 mol% the material is in the area of antiferroelectricity. Antiferroelectricity is very important in the application of this material and is described in the section 1.3 Electrical Properties.

1.1.1.3 Shannon Radii

Shannon radii are used as an estimate of the ion size in the material. They are a special kind of ionic radii with respect to coordination numbers. Furthermore a distinction between effective and crystal ionic radii is made. Effective ionic radii are listed to match Pauling´s radii, whereas the crystal ionic radii are closer to the physical size in the material. [11] Table 1 shows effective ionic radii, which have been used in this work.

Table 1- Ions with coordination numbers and corresponding ionic radii [12]

Ion	Coordination number	Ionic radius [Å]
Pb^{2+}	12	1.49
La^{3+}	12	1,36
Na^{+}	12	1.39
Cu^{1+} (extrap.)	12	1.25
Zr^{4+}	6	0.72
Ti^{4+}	6	0.605
Cu^{2+}	6	0.73
O^{2-}	4	1.38

1.1.1.4 Goldschmidt Tolerance Factor

In combination with Shannon radii the Goldschmidt tolerance factor is a useful tool to predict the symmetry/conformation of the structure. It gives information about the geometrical ratio between the ion`s radii in the perovskite structure on their lane of closest packing. It is given in Equation 1 with r_A = radius of the atom occupying the A site, r_B = radius of the B- atom and r_O = radius of the oxygen atom.

$$t = \frac{r_A + r_O}{\sqrt{2}(r_B + r_O)}$$

Equation 1 - Goldschmidt tolerance factor

The extent of the calculated tolerance factor yields information about the structure of the lattice. It can vary between hexagonal (> 1), cubic (~0.95 - 1), tetragonal (~0.95 - 0.9), rhombohedral (~0.9-0.85) and orthorhombic (~0.85-0.75). Below 0.75 the perovskite structure is usually instable. [13]

1.1.1.5 Copper and its Oxides

Copper was because of its noble character one of the first metals purified by the manhood (5000 B.C.). It is the lightest element in the group of the coin metals. In nature it is mostly found as Chalcopyrite ($CuFeS_2$) and Chalcocite (Cu_2S). Further

minerals where copper can be found in are hydroxides, chlorides, carbonates, oxides and ores containing also other metals. Metallic copper is very rare in nature.

The preferred oxidation states are 2+ and 1+. Moreover 0, 3+ and 4+ are possible too whereas 0 is only metastable at low temperatures. It is the second best electrically conductive metal following silver. High electro conductivity ($5.959*10^5\ \Omega^{-1}\ cm^{-1}$) and a much lower price than Ag/Pd makes it interesting for this certain application. Already traces of impurities decrease the conductance drastically. Therefore only highly purified copper is used for electrical applications. The typical cleaning procedure is done by dissolution in sulfuric acid on the anode and redepositon on the cathode in a galvanic bath. During this procedure nobler metals like Ag, Au, Pt sediment at the ground as anode mud and less noble metals like Zn, Sn stay in solution. Porous copper with purity above 99.95 % becomes deposited at the cathode.

As alternative electrode material in electro-ceramic materials copper was first investigated during the 60's. A melting point of 1083 °C requires lower sintering temperatures. Therefore the modification of the ceramic material by a sintering aid is necessary. Furthermore a close margin of stability between Lead oxide reduction and Copper oxidation depending on the oxygen partial pressure makes the process more challenging. In order to guarantee an exact adjustment of the oxygen partial pressure depending on the temperature, advanced process control is necessary.

Copper oxide is used in PZT based relaxors to reduce the sintering temperature. With the maximum densification at an amount of 0.7 wt.% CuO [14]. PbO-Cu_2O with an eutectic melting point of 680°C can also be used as liquid phase sintering assistant in $Pb(Zr_{0.52}Ti_{0.48})O_3$. 3 wt.% PbO-$Cu_2O$ help to reduce the sintering temperature from 1260 °C to 850°C [15]. Liquid phase sintering provides densification without additional grain growth in the material [16]. Avoiding the insertion of further dopants, except Cu/CuO keeps the material composition in the device simpler.

1.2 Defects

The concentration of defects is very important for the sintering behavior of a material as well as for its electrical properties. Higher defect concentrations in materials lead to faster diffusion and thereby to the reduction of the free surface energy which is the driving force for sintering processes. In other words defects in a material lower the sintering temperature. All defects in this chapter are described with respect to the PLZT material including the used dopants.

1.2.1 Intrinsic Defects

Intrinsic defects arise in a crystalline solid due to thermodynamic reasons. Therefore the total energy potential of the material becomes lower. Consequently at equilibrium a certain amount of defects is created depending on the temperature. This phenomenon can be described by Equation 2, with N_V the number of defects, N the number of sites in the lattice (number of potential defect sites), k the Boltzmann's constant and E_A the activation energy.

$$N_V = Ne^{\frac{E_A}{kT}}$$

Equation 2 - Defect equilibria in crystalline solids

1.2.1.1 Schottky Defects

One out of two known intrinsic defects is named as Schottky defect. Here, vacancies occur in pairs and the lattice atoms move to the surface (Equation 3). The crystal stays neutral, but the volume rises.

$$M_M + O_O \rightarrow V_M'' + V_O^{\bullet\bullet} + MO$$

Equation 3 – Schottky defect in a binary oxide in general

As a specific example for the PLZT system the following model is most favored. Lead oxide is moving to the surface (Equation 4) and evaporates due to its comparable low boiling point. Lead oxide depletion is avoided by addition of Lead oxide in a small excess to the powder mixture.

$$Pb_{Pb} + O_O \rightarrow V_{Pb}'' + V_O^{\bullet\bullet} + PbO$$

Equation 4 – PZT specific Schottky defect

1.2.1.2 Frenkel Defects

The second mechanism to introduce intrinsic defects is the incorporation of ions in between the lattice. Small ions are more likely to choose interstitial sites because of spatial reasons. (Equation 5)

$$M_M \rightarrow V_M'' + M_i^{\bullet\bullet}$$

Equation 5 – Frenkel defect in a binary oxide in general

In PZT, Titanium would be the ion of choice because it has the smallest radius. (Equation 6)

$$Ti_{Ti} \rightarrow V_{Ti}'''' + Ti_i^{\bullet\bullet\bullet\bullet}$$

Equation 6 – PZT specific Frenkel defect

1.2.2 Extrinsic Defects

Impurities in the material lead to extrinsic defects. On one hand pure commodities need to be used to gain products with predicted properties. On the other hand impurities are intentionally added as dopants to achieve the properties of materials (e.g. ion or electrical conductivity).

1.2.2.1 Acceptor Doping

Acceptor doping describes the replacement of ions by ions with a lower valency. To keep the crystal electrically neutral this is compensated by oxygen vacancies. Oxygen conducting properties are thereby improved.

In the material used in this work copper is regarded as acceptor dopant. (Equation 7)

$$CuO(s) \rightarrow Cu_{Ti}'' + O_O + V_O^{\bullet\bullet}$$

Equation 7 – PZT specific acceptor doping

1.2.2.2 Donor Doping

Cations with a higher oxidation state are incorporated as donors. This leads to the compensation by cation vacancies. (Equation 8)

$$Me_2O_3(s) \rightarrow 2Me_M^{\bullet} + 3O_O + V_M''$$

Equation 8 – Donor doping in general

In this thesis Lanthanum is added as donor. (Equation 9)

$$La_2O_3(s) \rightarrow 2La_{Pb}^{\bullet} + 3O_O + V_{Pb}''$$

Equation 9 – PZT specific donor doping

1.2.2.3 Donor Acceptor Neutralization/Elimination

If donors and acceptors are added to a material they compensate each other, reducing the number of vacancies. One cation with lower valency and one cation with higher valency have on average the same state of oxidation as the base cation. No vacancies or electrons are generated.

In the used material Copper and Lanthanum eliminate their function as acceptor/donor.

$$CuO + La_2O_3 \rightarrow Cu_{Ti}'' + 2La_{Pb}^{\bullet} + 4O_O$$

Equation 10 – Specific donor acceptor neutralization in PZT

1.2.2.4 Isovalent Doping

Isovalent doping enables the infinite solid solubility of two components as mentioned above. It entitles the displacement of a certain cation by another one owning the same valence. This procedure is charge-neutral and leads to infinite solubility (Equation 11).This opens the opportunity of the existence of certain systems as PZT, where Titanium is replaced by Zirconium or the other way around (Equation 12)

$$MeO_2 \rightarrow Me_M + 2\ O_O$$

Equation 11 – Isovalent doping in general

$$TiO_2 \rightarrow Ti_{Zr} + 2\ O_O$$

Equation 12 – PZT specific isovalent doping

1.2.2.5 Redox Equilibria / Oxygen Partial Pressure

The defect chemistry in ceramics is also influenced by the oxygen partial pressure of the atmosphere the ceramic is exposed to (Equation 13, Equation 14). Ions which own the property to change their charge are able to buffer the system.

$$O_O \leftrightarrow \frac{1}{2}O_2(g) + V_O^{\bullet\bullet} + 2e^-$$

Equation 13 – Formation of oxygen vacancies and free electrons through reducing atmosphere

$$\frac{1}{2}O_2(g) + V_O^{\bullet\bullet} \leftrightarrow O_O + 2h^{\bullet}$$

Equation 14 – Restocking of oxygen vacancies through oxygen rich atmosphere

1.3 Electrical Properties

Depending on the Zirconium/ Titanium/ Lanthanum content of PLZT ferroelectric and antiferroelectric materials can be gained.

1.3.1 Ferroelectricity

Materials with an electric dipole moment, which can be forced to change its direction by an external electric field, are named ferroelectrics. In such a material there are sections with different directions of this polarization, called domains. Before the polarization (applying an external electric field to the material) the material does not exhibit a macroscopic dipole moment. Poling leads to the growth of domains which already have had their polarization orientation in the direction of the applied field. Domains which are oriented rectangular to the field shrink, thus a macroscopic orientation is created. The material is polarized. After removing the external field a certain orientation of the dipoles remains, the so called remanence.

By adding dopants the electric behavior of the material can be tuned. Donors (e.g. La^{3+} substituting Pb^{2+}) induce a soft ferroelectric behavior (Figure 4). Acceptors (e.g. Mn^{3+} substituting Ti^{4+}) are accountable for a hard ferroelectric behavior. [17]

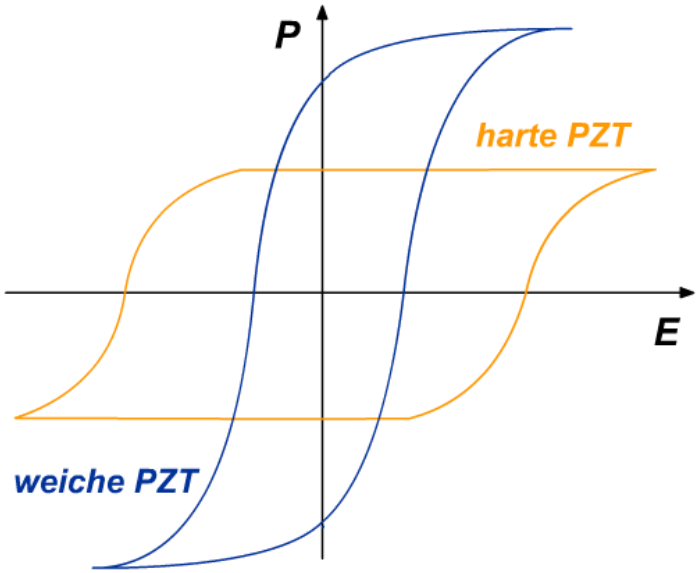

Figure 4 – Hysteresis loops of hard (yellow) and soft (blue) ferroelectric materials [18]

Soft materials have a high remanence and possess a relatively low coercivity, which means a high polarization remains and the electrical field which is needed to change the orientation is relatively low. A comparatively high loss emerges due to inner friction and a strong piezoelectric effect is observed. (Figure 4) Hard ferroelectric materials behave the other way around, showing a lower remanence and a higher coercivity. This leads to small losses and a weak piezoelectric effect.

1.3.2 Antiferroelectricity

Materials showing the effect of antiferroelectricity have unit cells with antiparallel aligned electric dipoles. The macroscopic dipole moment of a crystal without an external applied field is 0. During the polarization, dipoles in the crystals reorient themselves, to get as close as possible to the direction of the external applied field. At a certain voltage the dipole alignment changes from antiferroelectric to ferroelectric. This is visualized in the double hysteresis loop in Figure 5b. If this phenomenon is used in only one direction from the potential equilibrium it can be used in DC energy storage devices such as capacitors. If the voltage is removed and both electrodes become connected, power is released and the structure changes back to antiferroelectric. In PLZT with a high molar ratio of zirconia (>95 mol%) the antiferroelectric phase is stabilized [19]. With addition of Lanthanum the antiferroelectric phase is stabilized for even lower zirconia concentrations (Figure 3).

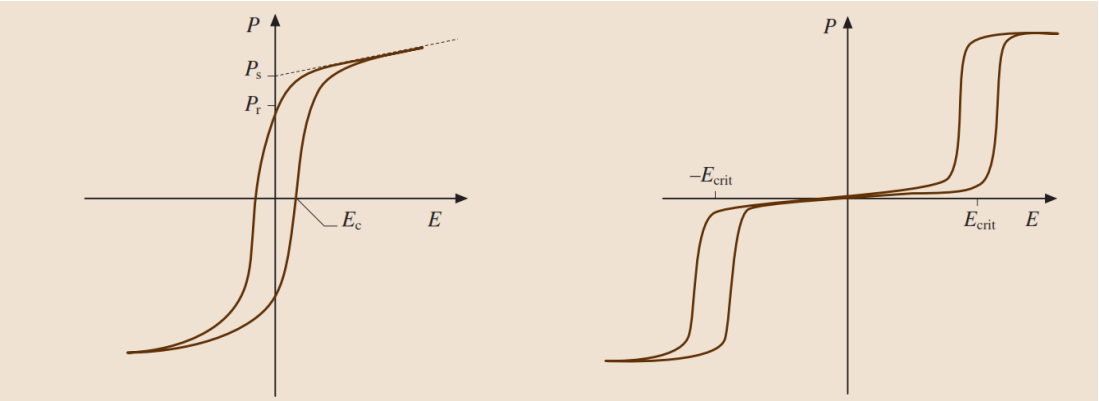

(a) (b)

Figure 5 – Single hysteresis loop of ferroelectric (a) material and double hysteresis loop through induced phase transition of antiferroelectric material (b) [20]

1.4 Aim

Precipitates in PLZT multilayer electroceramic components with copper electrodes were suspected to indicate the limit of solubility of copper oxide in the material. Therefore precipitates in the ceramics should be identified and the reason for their appearance should be clarified. Furthermore principles of copper incorporation into PLZT material and subsequent precipitation during processing should be investigated in dependence of the processing atmosphere and the copper content. Differences in defect chemistry and the limit of solubility should be discussed. The impact of the oxygen partial pressure in the atmosphere as process parameter on the resulting oxidation state of copper should be determined by XRD experiments and optical microscopy. The influence of the amount of copper oxide as sintering aid should be clarified by density determination. The influence on the microstructure should be monitored by scanning electron microscopy. Resulting properties of the material should be characterized by dielectric measurements.

2 Experimental

2.1 Material and Methods

2.1.1 Material

- PLZT powder with a Zr/Ti-ratio of 86/14 and a Lanthanum content of 7 mol% supplied by EPCOS OHG
- Copper(II)oxide powder (CuO) supplied by American Chemet

2.1.2 Methods

2.1.2.1 XRD experiments

The characterization by XRD experiments was done on a PANalytical X'Pert PRO MPD diffractometer. Measurements were performed on powder as well as on green and sintered bodies. Parameter Set 1 was used for ceramic powders, Parameter Set 2 was used for green and sintered bodies.

2.1.2.1.1 Parameter Set 1

Measurement parameters:	Bragg Brentano para focusing Theta/theta geometry X-rays: Cu $K\alpha_1$, $K\alpha_2$ Nickel filter Measurement in reflexion position Anti-scatter slit: 15 mm
Sample preparation:	Flat areas (diameter: 27 mm) prepared by the back loading technology

2.1.2.1.2 Parameter Set 2

Measurement parameters:	Bragg Brentano para focusing Theta/theta geometry X-rays: Cu $K\alpha_1$, $K\alpha_2$ Nickel filter Measurement in reflexion position Anti-scatter slit: 8 mm
Sample preparation:	Direct measurement of ceramic discs (diameter 10 mm)

2.2 Sample Preparation

2.2.1 Process Flow

The material under investigation is an inorganic oxide ceramic, made of the components Lead-, Lanthanum-, Zirconium- and Titanium oxide. The material itself was prepared through mixed oxide route, which is illustrated in Figure 6.

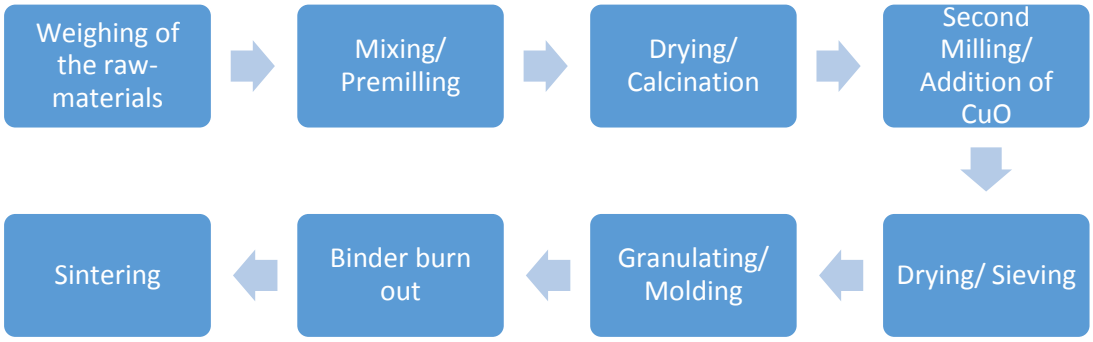

Figure 6 – Mixed oxide route (scheme)

Because of the supply of already calcined powder, this work starts at the point of second milling and addition of copper oxide as dopant.

2.2.2 Powder Mixing

At the beginning 20 different samples of PLZT powder containing different amounts of copper oxide (CuO), were prepared as listed in Table 2. The highest copper oxide quantity was chosen to be far above the expected saturation of the PLZT ceramic. The samples with lower copper oxide amounts were positioned around the expected solubility limit.

Table 2 - CuO content of the PLZT powder samples

Sample	CuO [mol%]	PLZT [g]	CuO [g]
		1st batch	
1	0.00	250	0.000
2	0.51	250	0.313
3	1.0	250	0.625
4	2.0	250	1.250
5	3.0	250	1.875
6	4.0	250	2.500
7	7.9	250	5.001
8	11.7	250	7.501
9	15.3	250	10.000
10	18.9	250	12.500
		2nd batch	
1	0.00	250.00	0
2	0.05	249.97	0.0313
3	0.10	249.94	0.0625
4	0.20	249.88	0.125
5	0.31	249.81	0.1875
6	0.41	249.75	0.2499
7	0.82	249.50	0.4999
8	1.2	249.25	0.7501
9	1.6	249.00	1.0001
10	2.0	248.75	1.2497

The samples were mixed in an eccentric ball mill, Retsch PM 100, using a beaker (1 L) and 500 g of 5 mm milling balls made from zirconia, at a speed of 100 rpm for 30 min in 250 g of water. Afterwards the suspensions were dried in a forced fresh air drying oven at 95 °C. The mixtures were sieved through a 315 µm sieve.

2.2.3 Granulating and Molding

100 g of each sample were merged with 15 g of 30 wt.% Polyethylene glycol solution, kneaded and dried for 30 min in a forced fresh air drying oven at 80 °C, sieved through a 315 µm sieve and dried for further 2 h under the same conditions.

About 50 disks, 15 mm in diameter and 1.37 -1.44 mm thickness were pressed from each sample.

2.2.4 Thermal Processing

Several discs of each series were processed under three different conditions:

- Binder burn out and sintering in air
- Binder burn out in air and sintering in reducing atmosphere
- Binder burn out and sintering in reducing atmosphere

2.2.4.1 Binder Burn Out

Binder burn out was done to remove organic components, which were needed during the molding procedure, before sintering. It was carried out in air as well as in reducing atmosphere.

2.2.4.1.1 Binder Burn Out in air

The binder was removed from the green bodies in a high temperature sintering furnace HTO 16/60 with an air flow of 20 L/min. The temperature was raised to 150 °C with a speed of 5 K/min, thereafter it proceeded with 3 K/min up to 370 °C, then with 1 K/min to 450 °C where it was held for 120 min and at the end it was cooled to room temperature with a rate of 5 K/min with external cooling (Figure 7).

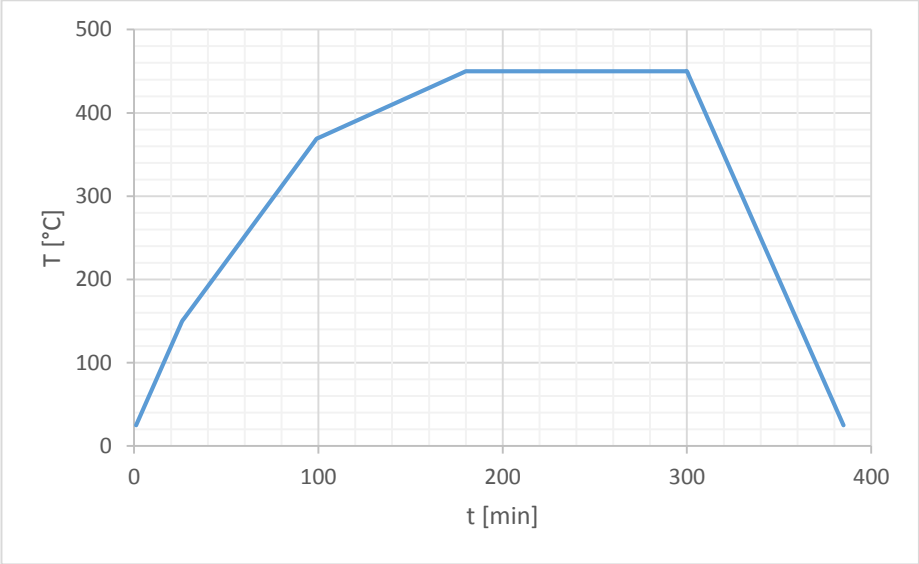

Figure 7 – Temperature program of the binder burn out treatment

2.2.4.1.2 Binder burn out under reducing atmosphere

The samples were processed in a debindering furnace under the same conditions as in the production to gain comparable results.

2.2.4.1.3 Redox experiments during the Debindering Process under Reducing Atmosphere

To get brief information about the behavior of copper(II)oxide during the debindering step of the process, each six already debindered pellets without and with 18.9 mol% CuO where weighed by an analytical scale before and after the debindering process. Already debindered samples were chosen to avoid uncertainty from an inexact amount of binder in the material. The exact amount of organics in each disk is not known because of inhomogeneous distribution of the binder in the powder.

2.2.4.2 Sintering

2.2.4.2.1 Sintering in Air

In the next working steps the debindered green bodies of each batch were stacked to towers. Zirconia sand was used to prevent the discs from sticking together. The furnace was heated with 3 K/min to 1050 °C. The temperature was held for 240 min and cooled down to room temperature with the same rate (Figure 8).

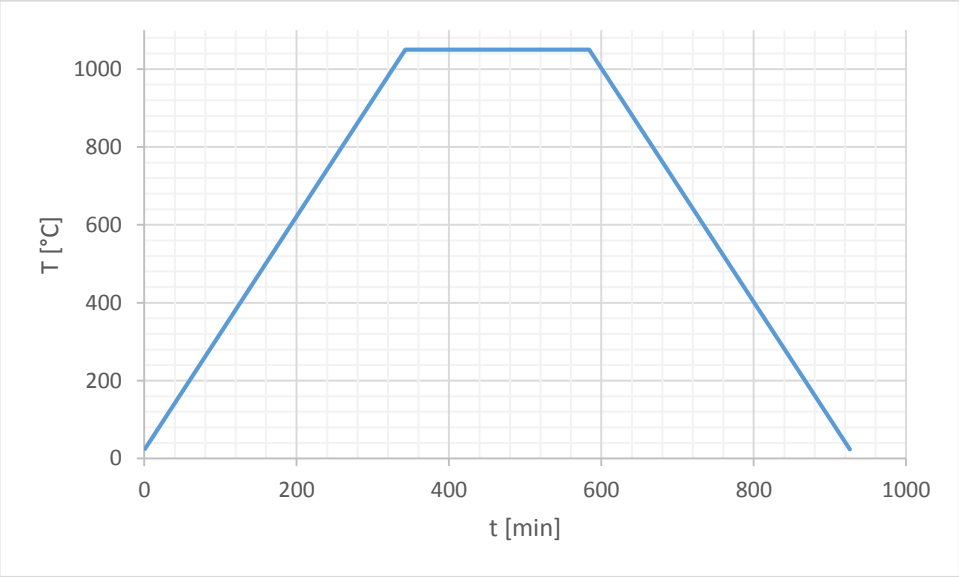

Figure 8 – Temperature treatment during the sintering process on air

After sintering the topmost and the bottommost discs were removed from the batch and discarded. As expected, the sample without copper oxide did not shrink as much as the ones containing copper oxide, which indicated incomplete sintering. Those having a copper content up to 0.3 mol%, showed a visible gradient in shrinkage and changes of color at the edges. That can be ascribed to the lead evaporation and copper diffusion during the thermal processing. Discs with a copper content of 0.4 mol% and higher were sintered to a relative density higher than 97 % and showed a very similar shrinkage behavior.

2.2.4.2.2 Sintering in Reducing Atmosphere

10 disks of each series were stacked to towers with zirconia powder in between. All samples were placed on a plate from MgO, covered with a MgO sleeve where a slit of 2 mm was left between cover and sleeve to allow the exchange of the atmosphere. Sintering under reducing atmosphere was performed in a rotary hearth furnace.

2.2.5 Preparation for Characterizations

2.2.5.1 Lapping

Six discs of each series were grinded to remove their surface which interacted with the atmosphere intensively. A cylindrical core having the dimensions of 10 mm in diameter and a height of 0.5 mm remained. The samples were cleaned in an ultrasonic aqueous bath and dried afterwards.

2.2.5.2 Cross Section Analysis

One sintered sample of each series was halved and casted in epoxy resin. Afterwards it was grinded and polished to prepare the surface for analysis of the cross section. To gain information about the structure of the sintered bodies, the prepared cross sections were treated by an etching solution, consisting of 100 mL H_2O + 1 mL HNO_3 + 2 drops HF. The time of the etching procedure was varied depending on the degree of sintering and observed according to satisfaction by light microscopy. Afterwards the samples were coated with carbon by high vacuum evaporation sputtering to create a conductive layer on the samples.

2.2.5.3 Metalizing

To contact the discs for the electrical measurement they were plasma magnetron sputtered under high vacuum provided by a turbo molecular pump. Three layers made from Chromium, Nickel and Silver were sputtered on the disk. A shadow mask with 8.2 mm in diameter was used in order to avoid the metallization of the edges and cylinder walls.

2.3 Characterization

2.3.1 Density

2.3.1.1 Geometrical Density

The geometrical density was determined by measuring the disks by slide gauge and weighing them.

2.3.1.2 Archimedes Density

Through weighing the samples in air and afterwards in water on the Archimedes scale the apparent density was obtained.

2.3.1.3 Theoretical Density

It was calculated by using the volume of the unit cell determined through XRD measurements and the average molecular weight of the ABO_3 structure.

2.3.1.4 Relative Density

By dividing the measured density through the theoretical density the relative density is calculated.

2.3.2 Scanning Electron Microscopy

The prepared samples, as described in 2.2.5 Preparation for Characterizations, were observed by a Jeol JSM 5900 with Tungsten filament cathode. They were transferred into the SEM and images of the microstructure in the material were taken.

2.3.3 Optical Microscopy

The cross section, prepared as described in 2.2.5 Preparation for Characterizations, was observed using an Olympus BX51M optical microscope by use of dark field imaging.

2.3.4 X-ray Diffraction

2.3.4.1 Powder Diffraction

All powders characterized were measured by pressing the loose powder into sample holders to provide a flat surface for the measurement.

2.3.4.2 Measurement on Sintered Samples

Flat, disc shaped samples were fixed on the sample holder by modeling clay. Therefore they could be measured without further preparation.

2.3.5 Gravimetrical Determination

To determine the weight loss during the reducing binder burn out, the samples were balanced on an analytical scale before and after the process.

2.3.6 Electrical Characterization

The polarization and the AC measurement with DC bias were performed by a FuG HCB 14M-12500 bipolar high voltage amplifier. The measurements were performed in Galden, a perfluorinated fluid of the Series HT110 produced by Solvay Special Polymers. A certain voltage program (see Figure 9, Figure 10) was applied to the disks and the resulting current was detected to get a charge/area vs. field strength diagram (Figure 29, Figure 30). From these signals the capacity was calculated with Equation 15 with the charge Q and the voltage U. The relative permittivity was gained using Equation 16, with the permittivity of the vacuum ε_0, the relative permittivity of the dielectric material ε_r, the area of the electrode A and the thickness of the dielectric layer d.

$$C = \frac{dQ}{dU}$$

Equation 15 – Calculation of the capacity of the samples during polarization

$$C = \varepsilon_r \varepsilon_0 \frac{A}{d}$$

Equation 16 – Capacity of a parallel plate capacitor

2.3.6.1 Polarization

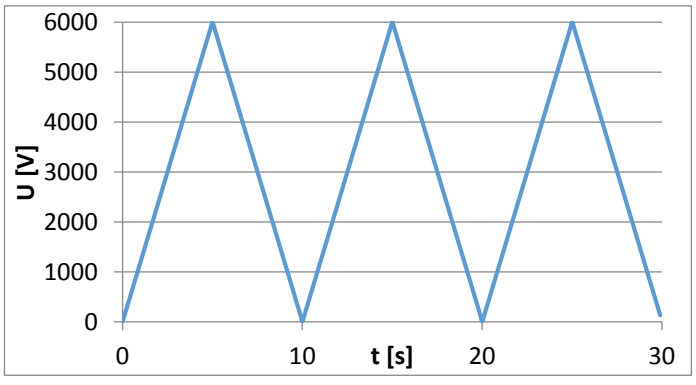

Figure 9 – Potential program of the polarization measurement

Polarization was performed at room temperature in transformer oil as viewed in the Figure 9. The large signal was gained from this measurement.

2.3.6.2 AC Measurement with DC Bias

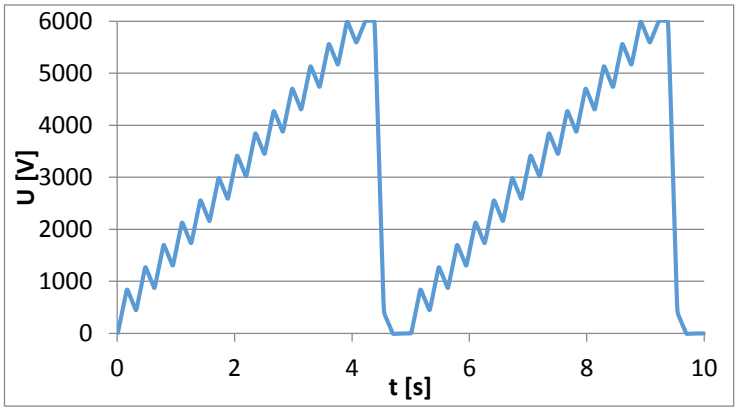

Figure 10 – Potential program of the Rippel test

This measurement is mentioned as Ripple test later on and the results named large signal with alternating bias were gained.

2.3.6.3 Capacity and Loss Factor

The capacitance was measured with a HP 4278A at 1 V and 1 kHz at room temperature.

3 Results and Discussion

3.1.1 Density

The density was determined by two different methods. The geometric dimension was measured by slide gauge and the density was calculated with consideration of the weight, the results of this method were called geometrical density. The Archimedes density was determined by weighing the samples in air and afterwards in water. Furthermore the relative density was calculated by dividing the absolute density through the theoretical density. Results are shown in Figure 11 and Table 2 - CuO content of the PLZT powder samples.

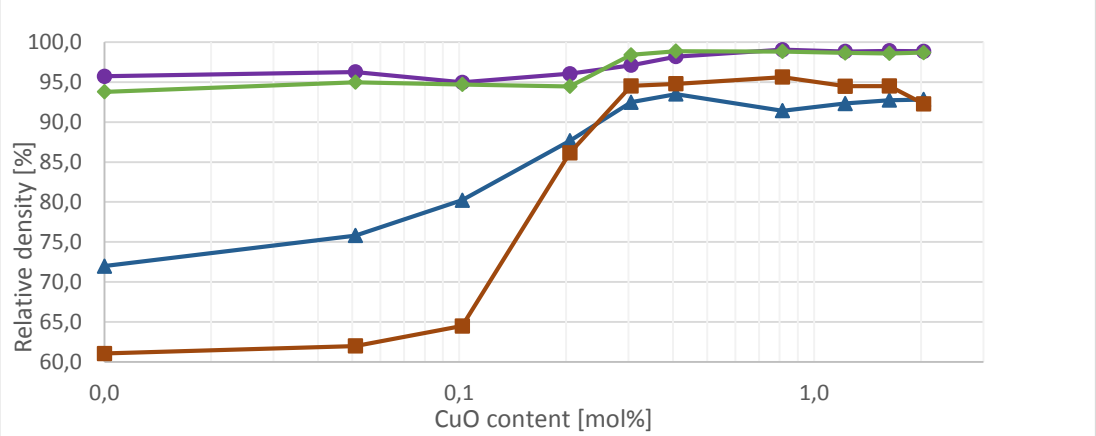

Figure 11 – Comparison of relative densities determined by the Archimedes method of samples sintered at 1050 °C in air (violet circles) and sintered under reducing conditions at 1030 °C (green chequer) and by geometrical determination of samples sintered in air (blue triangles) and samples sintered under reducing conditions (dark red squares) in dependence of the CuO content (the value 0.00 was changed to 0.01 to visualize it in the logarithmic scale)

Samples below 0.2 mol% CuO were not dense according to the geometrical density plotted in Figure 11. The differences between the geometrical density and the density measured by the Archimedes method up to a copper oxide concentration of 0.2 mol% can mainly be explained by open porosity. This was proven by a higher weight of the samples after immersing in water. Further deviations between these two methods occur due to imprecise caliper measuring and geometrical deviation from a perfect cylinder (compare geometrical and Archimedes densities above 0.3 mol%). Satisfying densification of the samples could be achieved at 0.3 mol% CuO and higher concentrations, where the relative density determined by the Archimedes method reached about 98%. The open porosity disappeared and a constant level of densification was reached. Furthermore, different sintering temperatures of the process in air at 1050 °C and in reducing atmosphere at 1030 °C might have influenced the result (compare geometrically determined densities below 0.3 mol% CuO).

Table 3 – Characterization of the sintered bodies

wt. % CuO	$wt._{loss}$ [%]	$d_{shrinkage}$ [%]	$h_{shrinkage}$ [%]	$V_{shrinkage}$ [%]	$\rho_{geometrical}$ [g/mL]	$\rho_{archimedes\ scale}$ [g/mL]	$\rho_{theoretical}$ [g/mL]	$\rho_{relative}$ [%]
Samples sintered in air								
0	0.90	7.8	9.6	24.7	5.573	7.412	7.743	95.73
0.051	0.77	10.1	10.9	28.5	5.861	7.444	7.732	96.27
0.102	1.04	11.2	13.1	32.8	6.197	7.334	7.724	94.96
0.205	0.71	12.9	15.7	38.1	6.766	7.414	7.719	96.04
0.305	0.79	16.0	16.7	41.8	7.138	7.494	7.718	97.10
0.408	0.76	16.8	17.3	43.0	7.217	7.579	7.719	98.19
0.815	0.64	13.8	17.7	41.6	7.056	7.645	7.719	99.04
1.225	0.96	15.3	17.7	42.5	7.125	7.626	7.716	98.83
1.63	1.08	15.0	17.7	42.5	7.153	7.628	7.713	98.90
2.035	0.73	14.1	17.7	41.8	7.155	7.620	7.709	98.85
Samples sintered under reducing conditions								
0	0.06	2.2	4.2	10.2	4.759	7.412	7.795	93.78
0.051	0.20	2.6	4.7	11.6	4.832	7.444	7.795	94.98
0.102	0.17	3.1	5.9	14.1	5.022	7.334	7.788	94.70
0.205	0.32	11.3	15.5	36.7	6.681	7.414	7.741	94.46
0.305	0.15	14.4	17.2	41.3	7.303	7.494	7.726	98.42
0.408	0.34	14.9	17.3	41.8	7.325	7.579	7.727	98.87
0.815	0.09	15.5	17.4	42.4	7.387	7.645	7.725	98.83
1.225	0.14	14.5	17.3	41.9	7.297	7.626	7.723	98.65
1.63	0.17	15.0	17.3	41.8	7.295	7.628	7.720	98.59
2.035	0.06	12.8	17.2	40.2	7.116	7.620	7.711	98.69

The sintered bodies were characterized and compared to the green ones. A small deviation might have occurred through lead evaporation during the process. Therefore the theoretical density might have changed.

3.1.2 X-ray Diffraction

3.1.2.1 Determination of the Limit of Detection

The aim of these measurements was to figure out the limit of detection in mixtures of copper oxide and PLZT conversion powder.

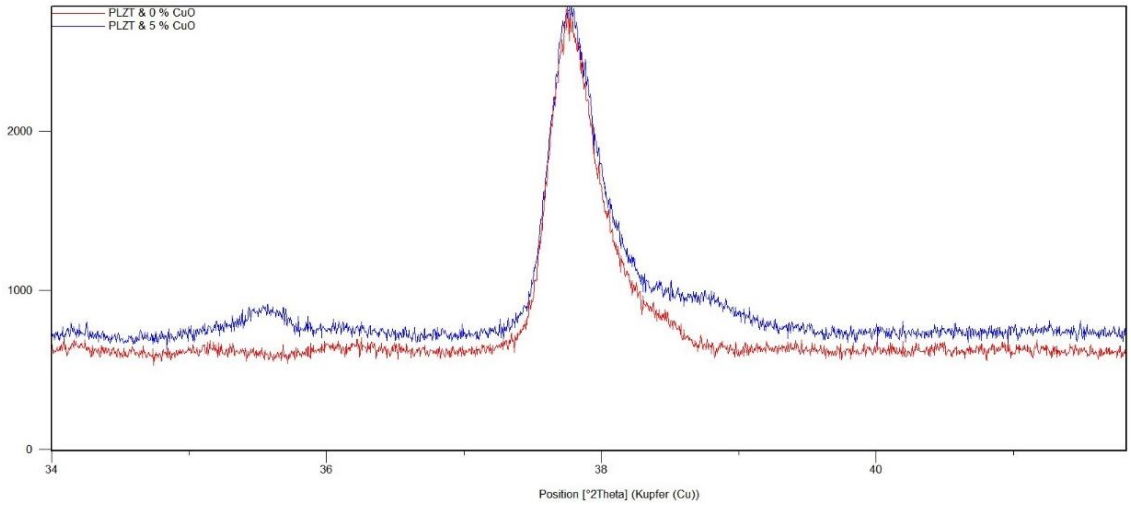

Figure 12 – Differences in the XRD pattern between PLZT without (red line) and containing 18.9 mol% CuO (blue line)

The area between 35.2 and 35.9 °2Theta ((002) Peak at 35.56, 96.4 %) in Figure 12 was chosen to quantify the CuO content. The area between 38 and 40 °2Theta ((200) Peak at 38.754, 100 %) is less expressive because of overlay with the (111) peak of PLZT.

In Figure 13 the appearance of the (002) peak of CuO in the XRD pattern is visualized. Looking at the lines a Limit of Detection at about 1 wt.% CuO (4.1 mol% CuO) can be regarded as justified. Going deeper in detail, by integrating the areas between 35.2 and 35.9 °2Theta and subtracting the blank this first impression was confirmed.

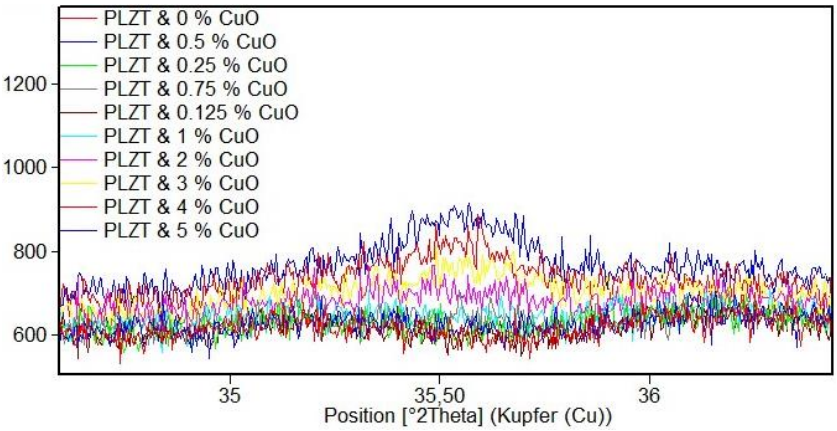

Figure 13 – Impact on the XRD pattern due to a varying copper content

Looking at the diffractograms (Figure 13) and the correlation of the peak area to the copper oxide content in Figure 14 the **Limit of Detection** of the copper oxide content in the samples is at about **4 mol%** (1 wt.%). Quantification at lower concentrations is not possible in this case.

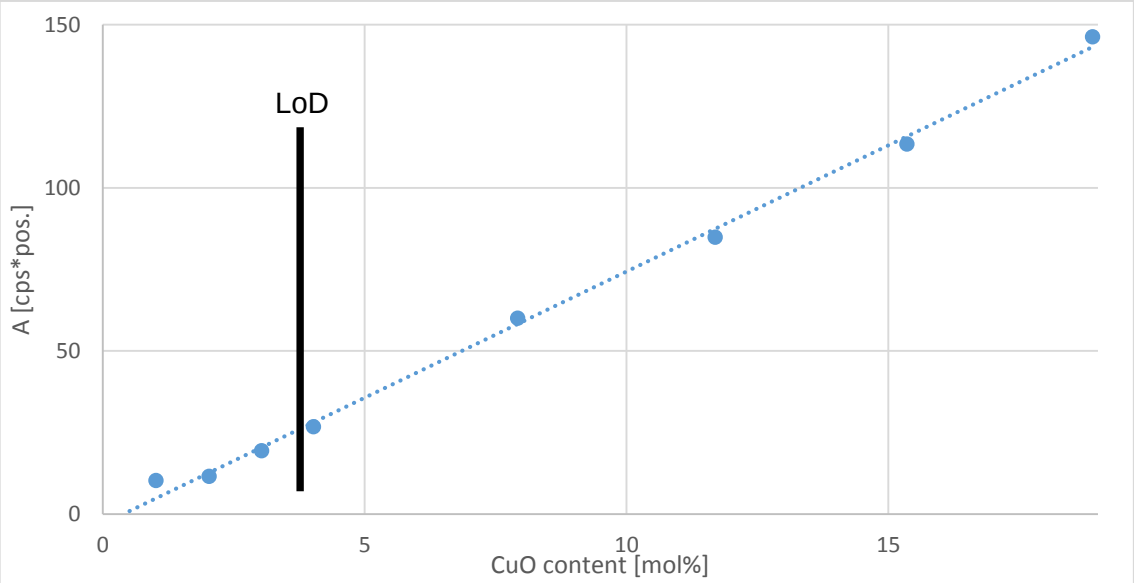

Figure 14 – CuO content vs. peak- area of the XRD signal with the Limit of Detection (black)

This result shows that this method is not applicable for detection of CuO as secondary phase, since the copper content in most of the samples is below the LoD.

3.1.2.2 X-ray Diffraction on Sintered Bodies

In a first trial the same material before and after grinding was examined to check out changes in the material through the mechanical treatment. As already expected significant differences could be identified (Figure 15, Figure 16). Grinding causes “mechanical poling” and therefore a preferred orientation of polarization. This leads to changes of the intensity of the reflexes in the diffractogram. To reduce the effect of preferred orientation, grinded samples were tempered. But tempering caused segregation of lead oxide and obviously changed the composition of the perovskite. Furthermore the oxidation of copper and copper(I)oxide during tempering eliminated the usefulness of this method. The correction of the preferred orientation was done by mathematical operations instead.

As visualized in Figure 15 and Figure 16 tempering at 430 °C leads to slight changes in the spectra and in the color due to oxidation of copper oxide in the samples. The treatment at 700 °C results in several additional peaks in the pattern, which were caused by degradation during tempering. Those peaks (Figure 16) were identified as reflections of Massicot and Litharge, the two polymorphs of lead(II)oxide.

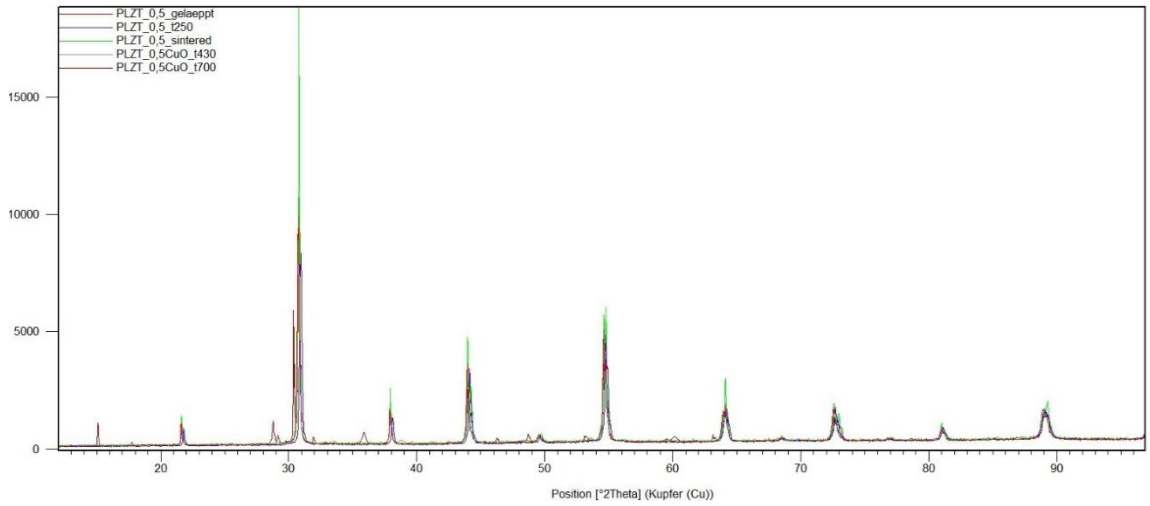

Figure 15 - Differences in the XRD pattern of PLZT + 0.5 wt.% (2 mol%) CuO before mechanical treatment (green line), after mechanical treatment (red line), after temperature treatment at 250 °C (blue line), after treatment with 430 °C (grey line) and after treatment at 700 °C (brown line)

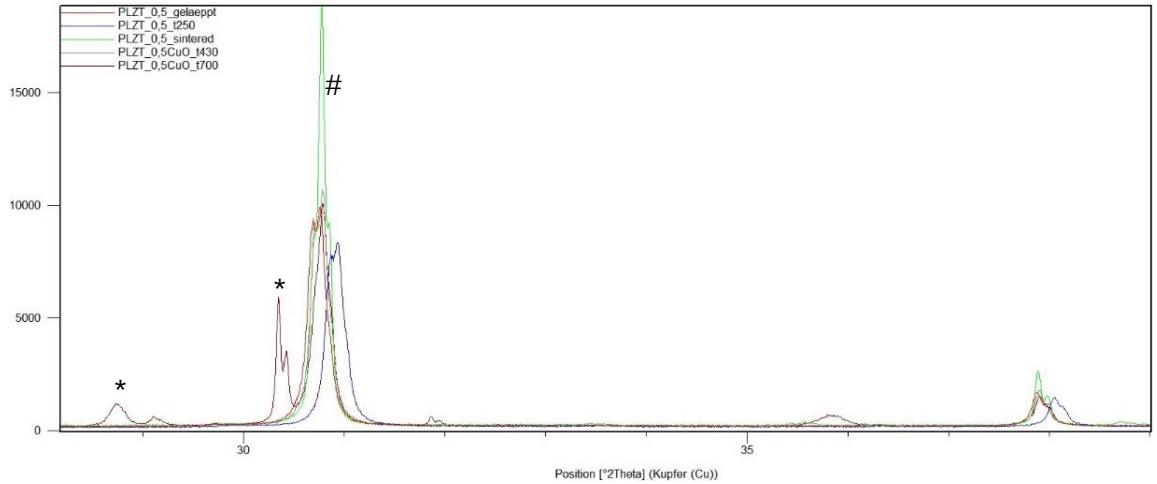

*Figure 16 – Zoomed cleavage of differences in the XRD pattern of PLZT + 0.5 wt.% (mol%) CuO before mechanical treatment (green line), after mechanical treatment (red line), after temperature treatment at 250 °C (blue line), after treatment with 430 °C (grey line) and after treatment at 700 °C (brown line); *reflexes from β-PbO, Massicot , #different reflex shape induced by mechanical stress*

The changes of the color which are shown in Figure 17, occur through oxidation of copper(I)oxide to copper(II)oxide.

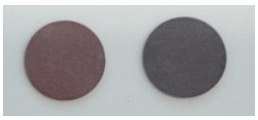

Figure 17 – Visual color change of the material during tempering at 430 °C in air of a PLZT ceramic, containing 0.5 wt.% (2 mol%)CuO

Due to those changes of the sample during thermal processing, the decision was made to take XRD spectra without any pretreatment.

To check out the depth of this oxidation process one of the samples was grinded at its surface and observed through XRD once more. (Figure 18)

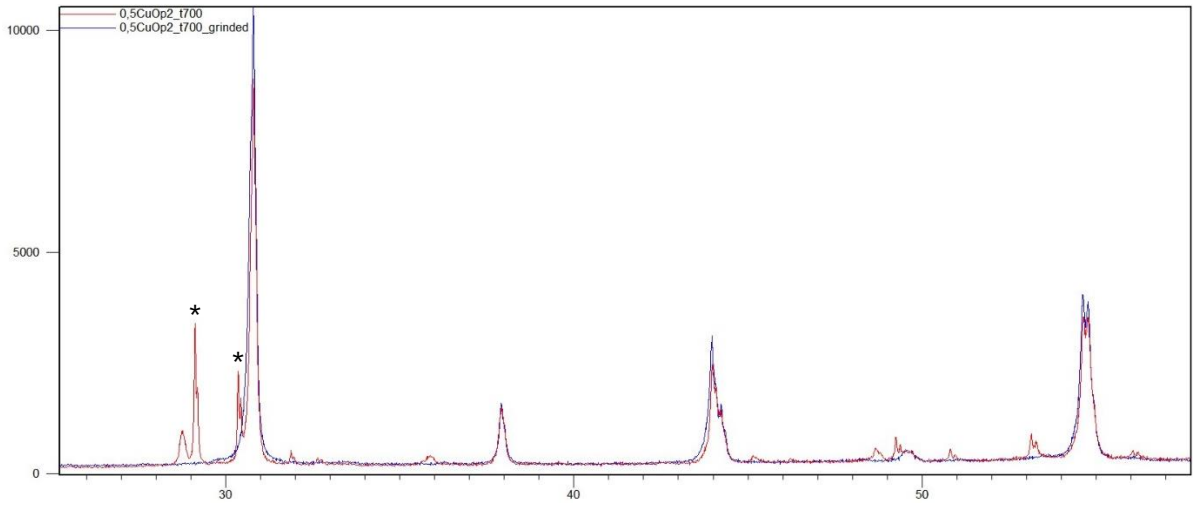

*Figure 18 – Difference between the pattern of a PLZT containing 0.5 wt.% CuO before (red line) and after grinding (blue line); *reflexes from PbO*

Due to the difference in the patterns the PbO enrichment only at the surface is proven. After grinding few microns off the surface the PbO was not found any more in the pattern. This procedure was not done to the samples where the lattice constants were determined, since the PbO on the surface is a sign of specimen variance.

3.1.2.2.1 Dimensions of the Unit Cells determined by XRD

To get information about the behavior of copper ions in the material, the lattice constants of the perovskite phase were calculated. Furthermore dependencies between the amount of copper in the sample and the unit cell volume was visualized in Figure 19.

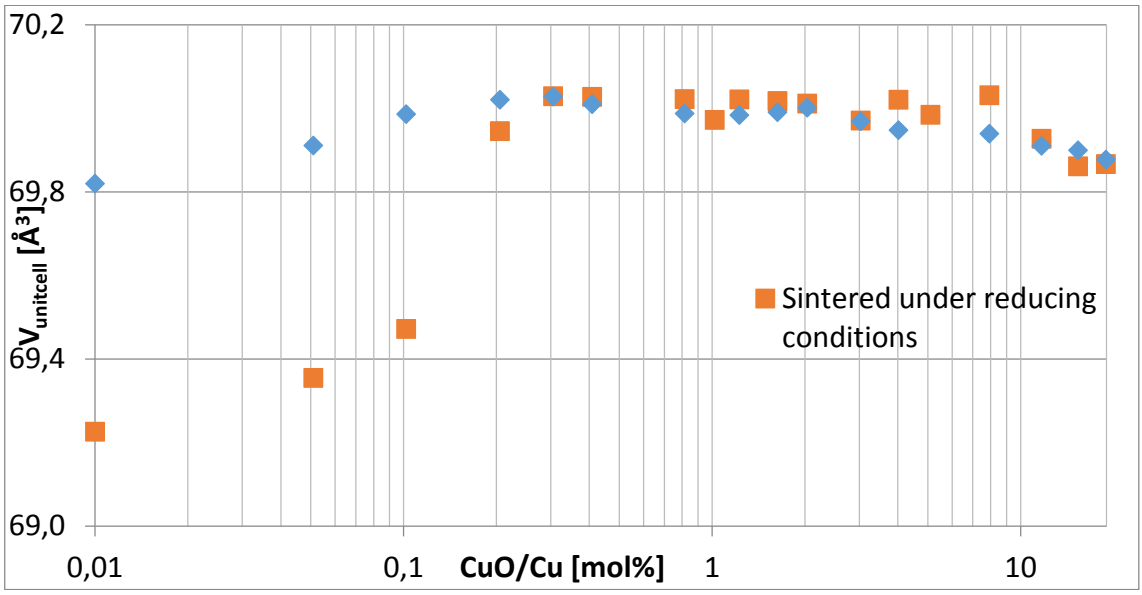

Figure 19 – Unit cell volume vs. Cu content (the value 0.00 was changed to 0.01 to visualize it in the logarithmic scale)

The influence of Copper Oxide on the unit cell can be described by the incorporation of the Cu^{2+} ion into the Lattice. With an ionic radius of 0.73 Å Cu^{2+} is bigger than Zr^{4+} (0.72 Å) and Ti^{4+} (0.605 Å). Therefore the size of the unit cell rises due to Cu^{2+} incorporation on the B site. If Copper Oxide would be provided as Cu_2O to the lattice it would be more favored to occupy the A site due to the low ionic charge and an ionic radius of 1.25 Å. Considering the ionic radius of Pb^{2+} (1.49 Å), La^{3+} (1,36 Å) and Na^{+} (1.39 Å) this opportunity would lead to a decrease of the unit cell volume.

The volume of the unit cell in Figure 19 has a maximum at 0.3 mol%. The growth of the unit cell can be explained by the incorporation of the Cu^{2+} ion on the B-site. The copper ion has a bigger radius than Ti^{4+} and Zr^{4+}. After the maximum size of the unit cell the copper incorporation seems to stop and the unit cell volume starts to decrease again at 0.4 mol% CuO. Additional occupation of A-sites by Cu^{+} or the depletion of Cu^{2+} in the perovskite phase by the additional Tenorite phase (CuO) could explain the decrease of the unit cell volume. This cannot be decided on the basis of the available data.

3.1.2.3 Influence of the Process on the material visualized by XRD

XRD investigations on samples with a CuO content of 19 mol% helped to visualize the effect of the thermal process on the redox behavior of copper oxide in the samples. This amount of copper oxide as dopant is not common and was just used to get an idea about the redox reactions in the material

Depending on the debindering and sintering conditions CuO, Cu_2O and metallic Cu can be found in pattern of the material (Figure 20, Figure 21). Debindering and sintering in air results in CuO, debindering in air and sintering under reducing conditions leads to Cu_2O in the material and debindering and sintering under reducing atmosphere causes the formation of metallic copper in the material.

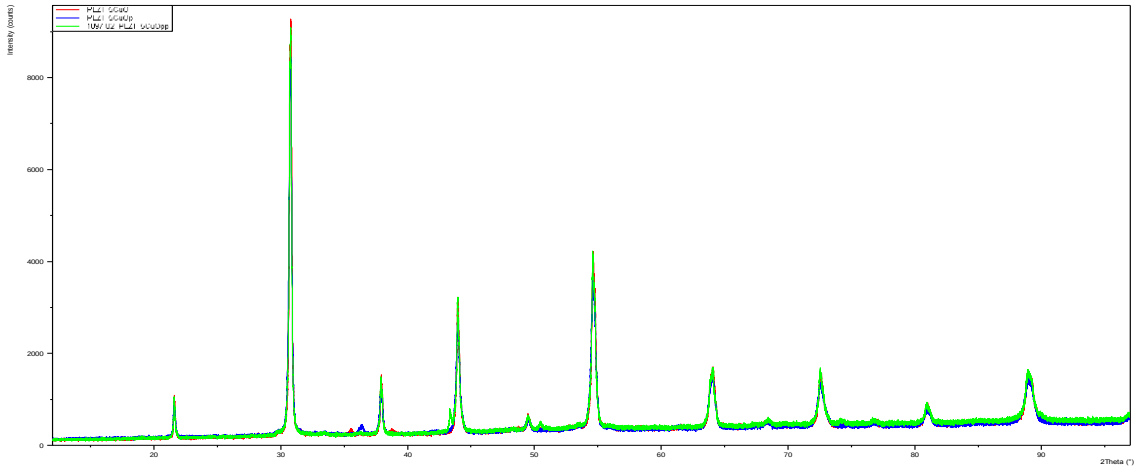

Figure 20 – XRD pattern of PLZT + 19 mol% CuO

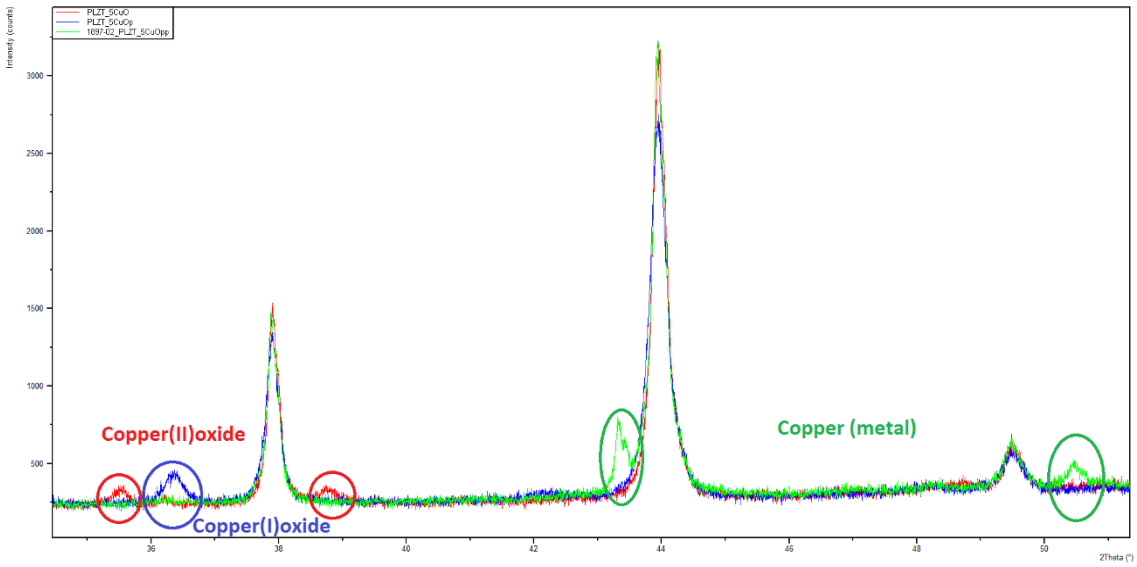

Figure 21 – Magnified section of XRD pattern of PLZT + 19 mol% CuO processed in air (red), debindered in air and sintered in reducing atmosphere (blue) and processed under reducing conditions (green)

3.1.3 Copper Oxide Reduction during Binder burn out process

To investigate the reduction of CuO, samples with 19 mol% CuO debindered in air, subsequently underwent the process of binder burn out under reducing conditions. By that it was ensured, that the oxidation state of copper before the binder burn out under reducing conditions was +II. For a reduction of CuO to Cu_2O a weight loss of 0.51 wt.% is expected. For the complete reduction of CuO to metallic Cu in the samples a weight loss of 1.01 wt.% would result. The weight loss of disks with 19 mol% CuO was 1.07 wt.%. Taking into account the weight loss of a PLZT disk without CuO under the same conditions, which is 0.11 wt.%, yields a corrected weight loss of 0.96 wt.%. This means 95.5 wt.% of the CuO in the samples was reduced to metal copper.

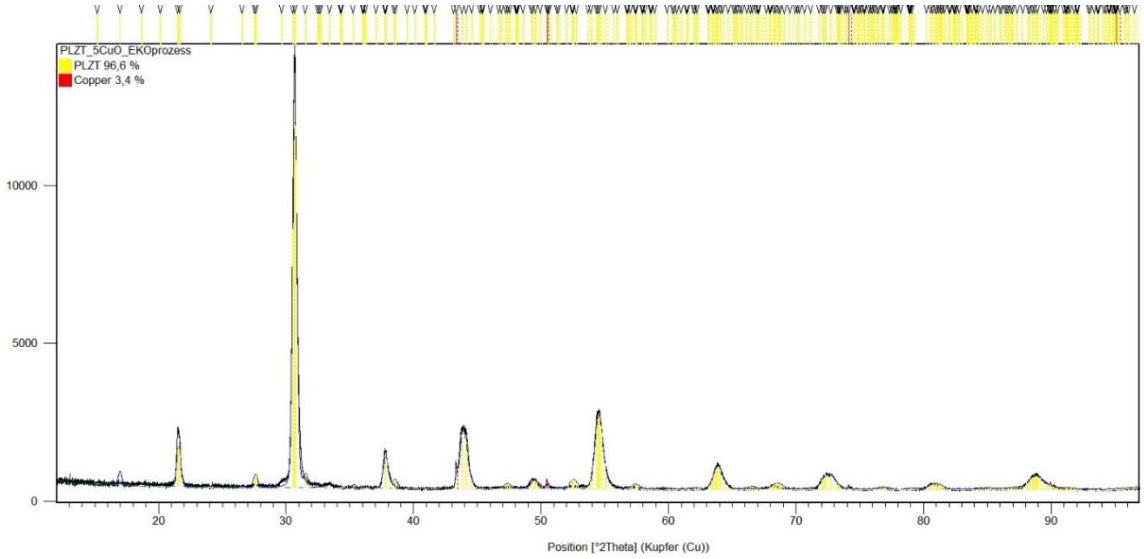

Figure 22 – XRD pattern of reducing debindered PLZT + 19 mol% CuO pellets

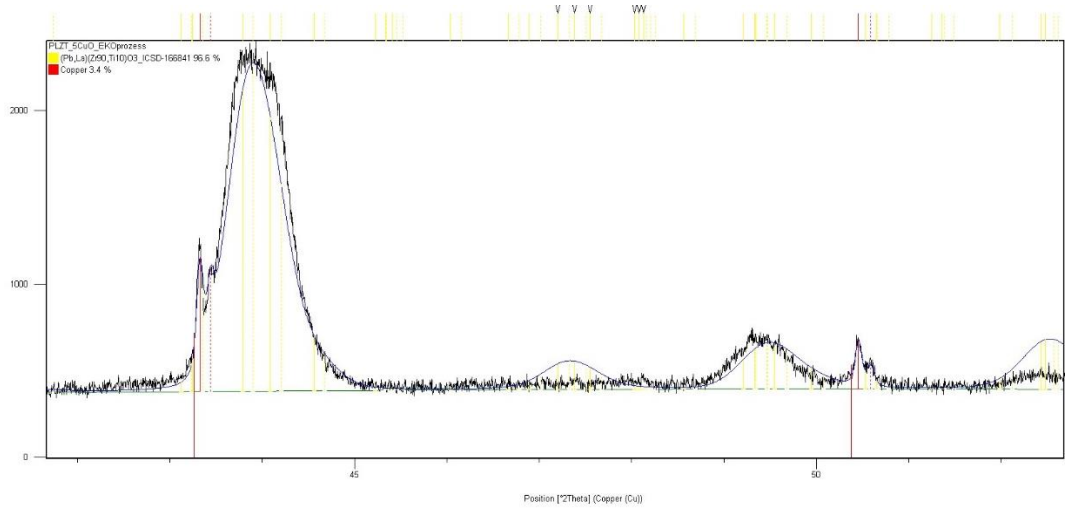

Figure 23 – Selected area of XRD pattern of reducing debindered PLZT conversion powder + 5 wt.% CuO pellets

Figure 22 and Figure 23 confirm the results of the gravimetric determination, that the copper oxide was reduced to metallic copper (red lines in the spectra).

According to the gravimetric and XRD results it is proven, that CuO is being reduced to metal copper. An amount of 0.93 mol% which is migrating into the grains stays in the lattice as CuO or Cu_2O.

3.1.4 Scanning Electron Microscopy

The images in Figure 24 show the effect of etching on the analyzed samples. The identification of the grain boundaries becomes possible by etching.

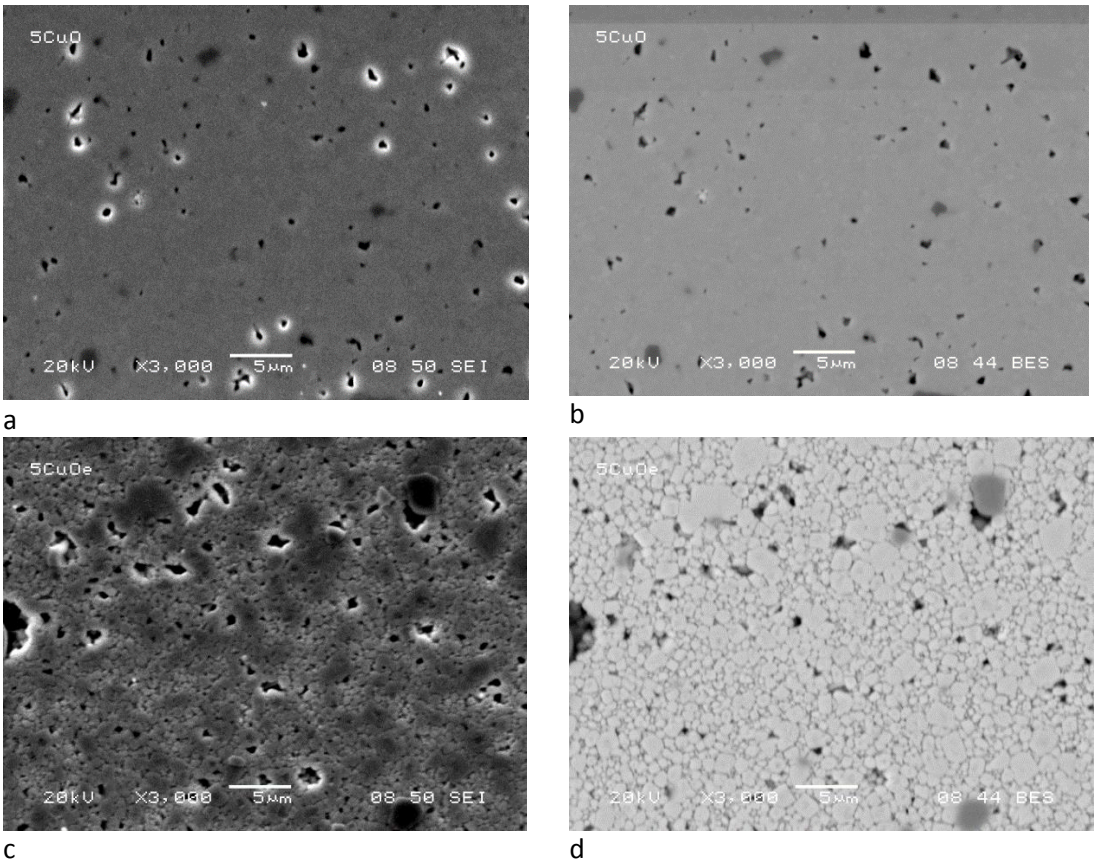

Figure 24 – Images of PLZT containing 19 mol% CuO taken by Scanning Electron Microscopy before (a) – SEI , (b) – BEI and after etching (c) – SEI, (d) – BEI

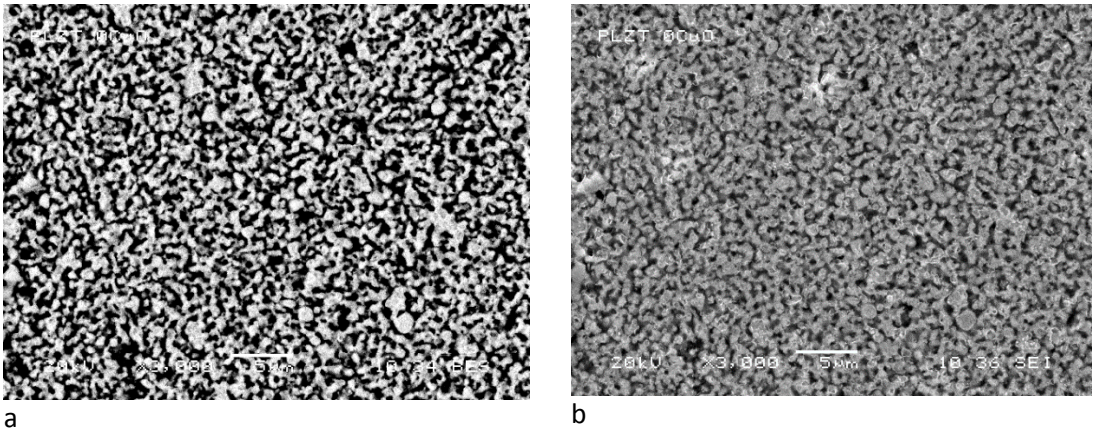

Figure 25 – Scanning Electron Microscopy pictures of disks sintered without copper BEI (a) and SEI (b)

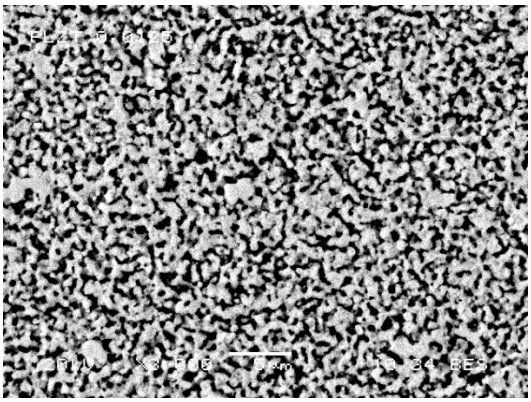

1a

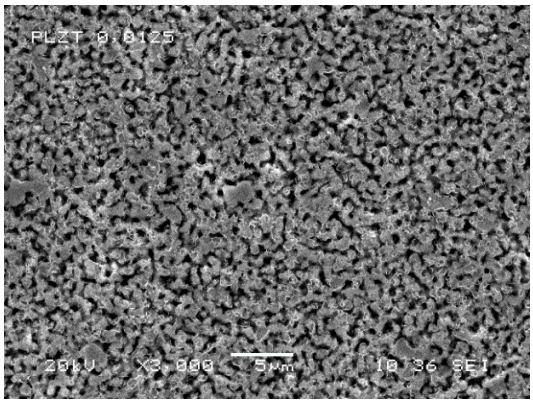

1b

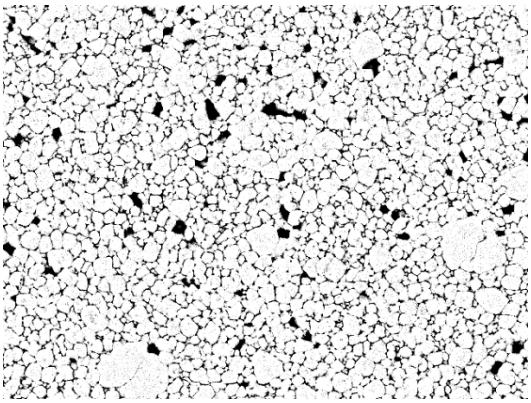

2a

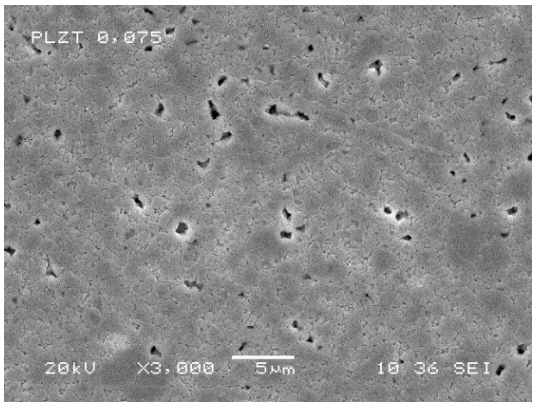

2b

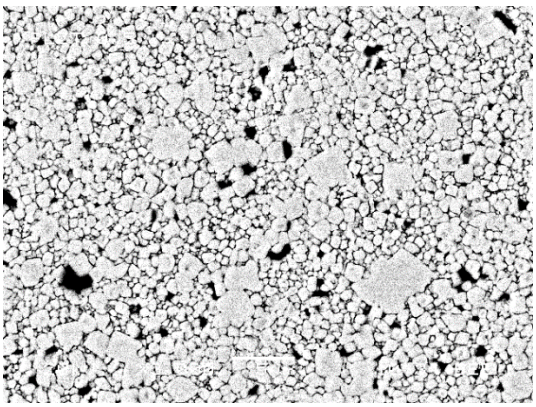

3a

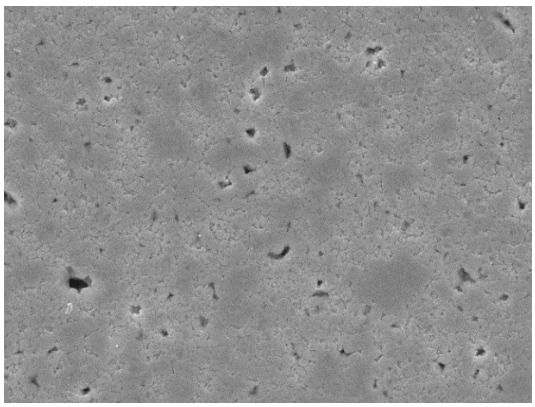

3b

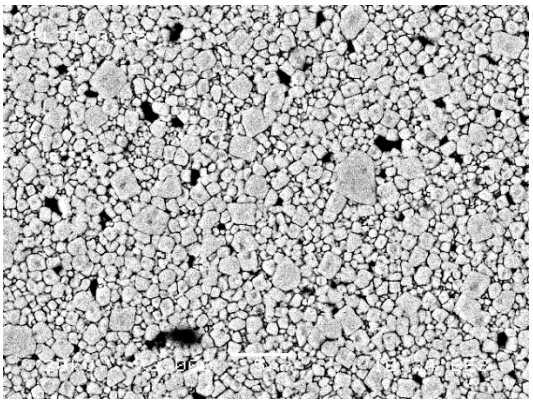

4a

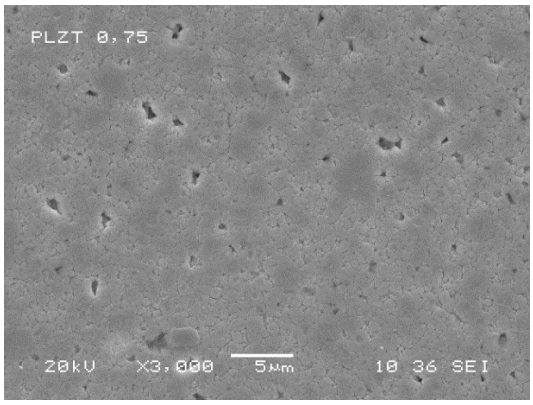

4b

Figure 26 – Scanning Electron Microscopy pictures of disks sintered with 0.05 mol% copper oxide BEI (1a) and SEI (1b), 0.3 mol% BEI (2a) and SEI (2b), 2 mol% BEI (3a) and SEI (3b), 3 mol% BEI (4a) and SEI (4b)

Figure 26 and Figure 26 show SEI and BEI images of sintered and etched PLZT samples with different CuO contents. At concentrations below 0.075 wt.% (0.3 mol%) CuO, sintering does not perform satisfyingly. For the chosen sintering conditions the samples are porous. At 0.075 wt.% (0.3 mol%) and above the samples are homogeneously densified and have similar grain size distributions.

This confirms copper oxide as sintering aid as already mentioned in 3.1.1 Densit. Furthermore copper oxide works as liquid phase sintering assistant and therefore does not influence the grain growth during sintering (1.1.1.5Copper and its Oxides).

3.1.5 Optical Microscopy

In Figure 27 dark field images taken by an optical microscope are imaged. Samples with different copper concentrations sintered in air and under reducing conditions are represented.

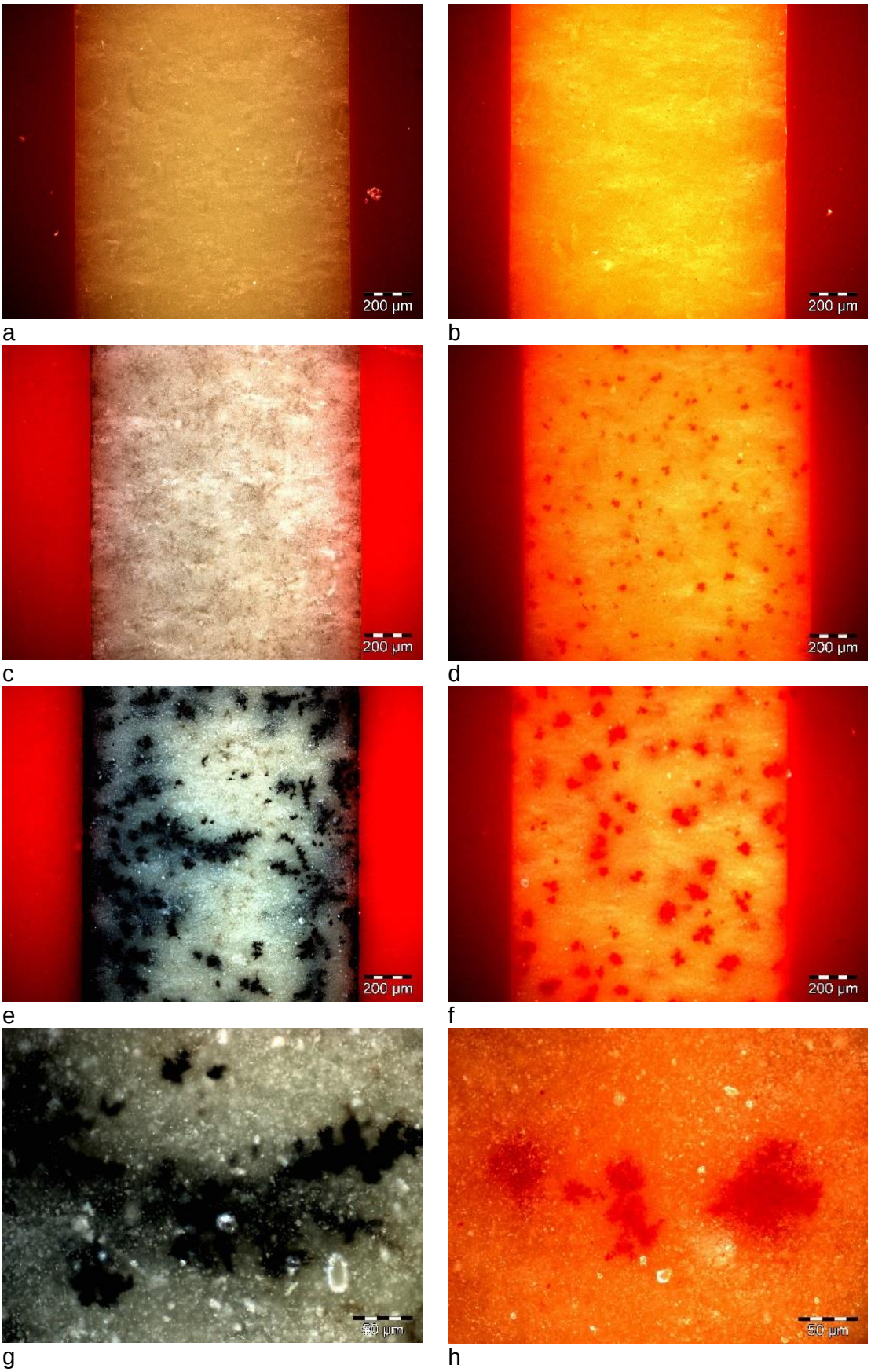

Figure 27 – Dark field images taken by a light microscope showing samples with a copper content of 0.3 mol% processed on air (a) and under reducing conditions (b) 0.4 mol% processed on air (c) and under reducing conditions (d), a copper content of 2 mol% sintered on air (e,g) and sintered under reducing conditions (f,h)

In the dark field images in Figure 27 red spots (most probably Cu_2O) in the samples processed under reducing conditions, and grey/black spots (most probably CuO) in the samples sintered in air, were detected for CuO concentrations more than 0.3 mol%. These findings indicate the solubility limit of Cu_2O and CuO, respectively in PLZT.

One theory to explain the segregation of the copper oxide is to consider a higher solubility of the oxides at higher temperatures. During the cooling after the sintering process the solubility decreased and the oxides segregate at random spots in the ceramic. This happened at a CuO content of 0.3 mol% and higher concentrations. With increasing CuO addition the spots start to grow as a three dimensional structure between the grains like dendrimers. Since the amount and size of the copper oxide precipitates in the samples sintered in air and under reducing conditions has been similar, an analogous solubility behavior is supposed.

A quantification of the area occupied by Cu_2O precipitates (red spots in the pictures) was done (Figure 28) with the picture processing program analySIS auto.

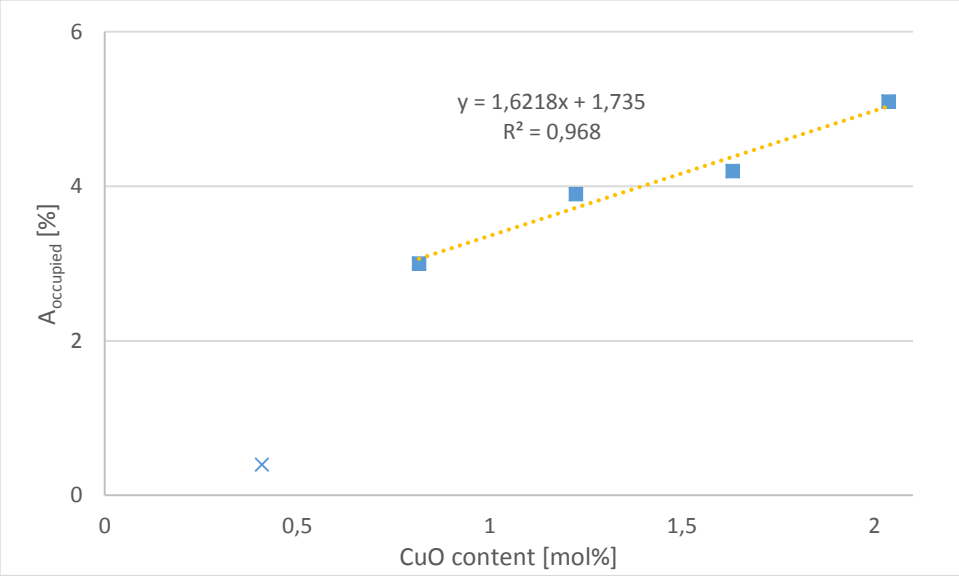

Figure 28 – Quantification of the Cu_2O excretions by the area

Figure 28 shows the correlation between the copper content of the samples and the area occupied by the colored precipitations. By this correlation a quantitative statement on the amount of copper oxide in the material in a concentration area from 0.8 until 2 mol% can be made. The crystallographic unit cell has its maximum size at 0.3 mol% where the incorporation of copper ions into the crystal lattice stops. At an amount of 0.4 mol% CuO the first precipitates were perceived, more copper oxide in the material leads to more and bigger precipitates

Differences in the brightness of the pictures induced a certain mistake into the quantification. Especially color differences of the sample below 0.8 mol% lead to difficulties (blue cross in Figure 28). The area with higher CuO concentration is close to linearity.

3.1.6 Electrical Characterization

The polarization measurements were carried out as described in 2.3.6 Electrical Characterization. The curves showed a slight drift because of a leakage current. This offset was mathematically corrected and closed loops were obtained. This procedure was done to eliminate mistakes in the calculation of the area of the hysteresis as well as in the comparability of the measurements.

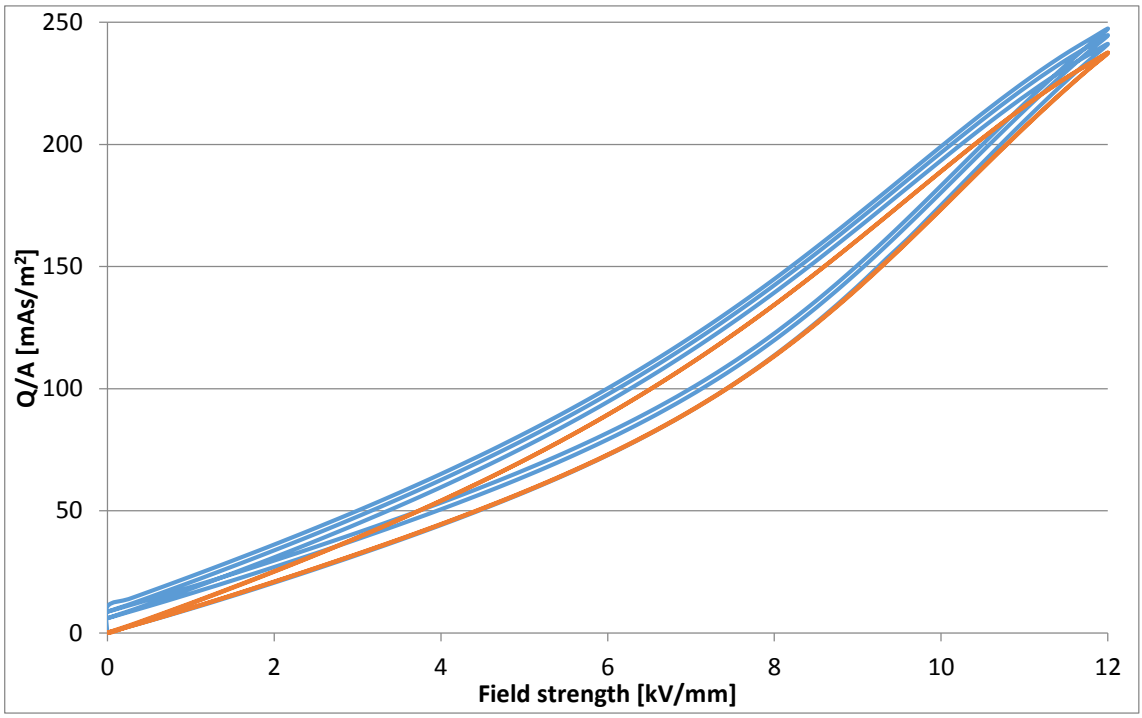

Figure 29 – Charge/Area vs. Field strength (blue curve) and a corrected curve (orange line)

During the polarization (Figure 29) a reversible transition from antiferroelectric to ferroelectric ordering is induced at the so called switching field (10 kV/mm for a sample containing 1.2 mol% CuO shown in Figure 29). This reversible phase transition can be used for charge storage at high electric fields. Furthermore the height of the sample elongated about 0.12 % (500 µm to 500.6 µm). This elongation causes stress in the material.

The area of the loop represents the loss which is a result of the heating of the material through the inner friction during the orientation and reorientation in the lattice.

The signal from the Ripple test was corrected the same way to eliminate the mistake induced by leakage current (Figure 30).

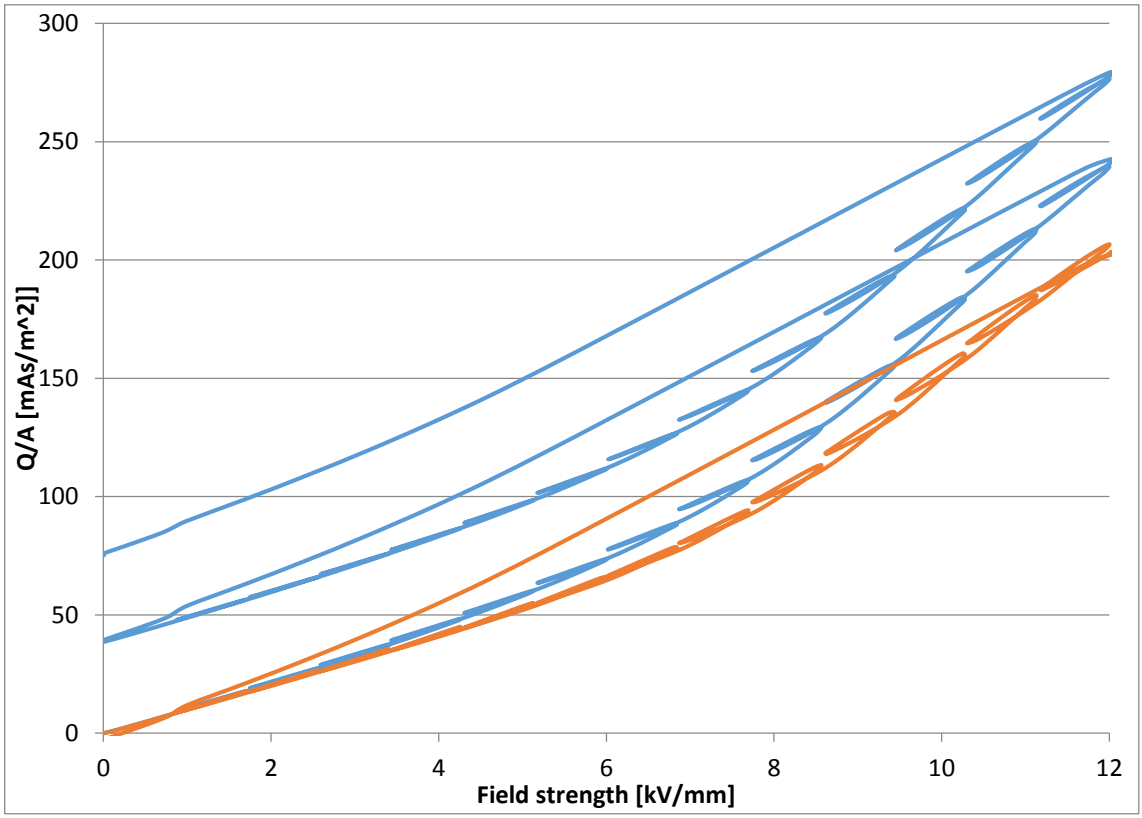

Figure 30 - Measured (blue line) and corrected signal (orange line) of the Ripple test

The large signal was provided by the polarization and the large signal with alternating bias was received from the Ripple test.

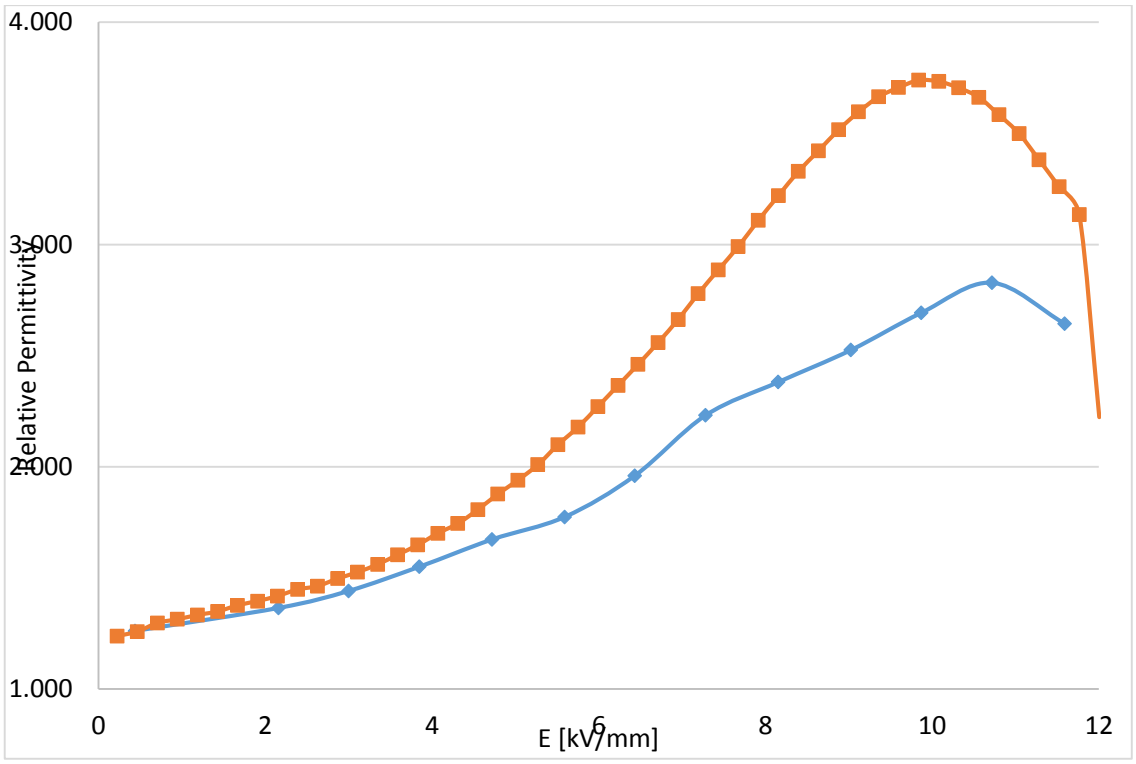

Figure 31 – Relative Permittivity of the large signal (orange line) and the large signal with alternating bias (blue line) vs. the electric field

Conclusively, the maxima of each curve in Figure 31 were plotted versus the copper content.

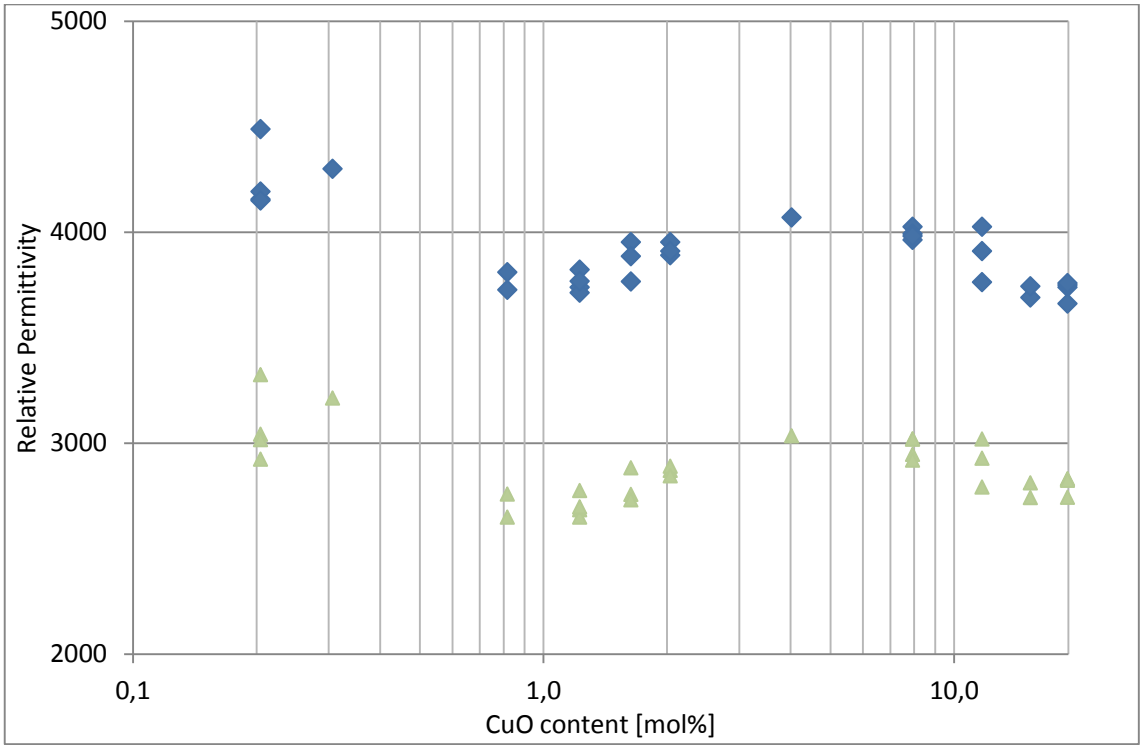

Figure 32 – Relative permittivity obtained from the large signal (blue squares) and from the large signal with alternating bias (green triangles) vs. CuO content

As visualized in Figure 32 the relative permittivity was not shifted significantly, nor was the switching field shifted to higher or lower field strength. It was not possible to gain values from disks with lower CuO contents than 0.2 mol%. Sintering of samples having a CuO content lower than 0.2 mol% did not proceed satisfyingly within the chosen sintering temperature because of too little sintering aid (CuO). All samples containing 0.4 mol% did not stand the characterization due to high elongation and stress in the material.

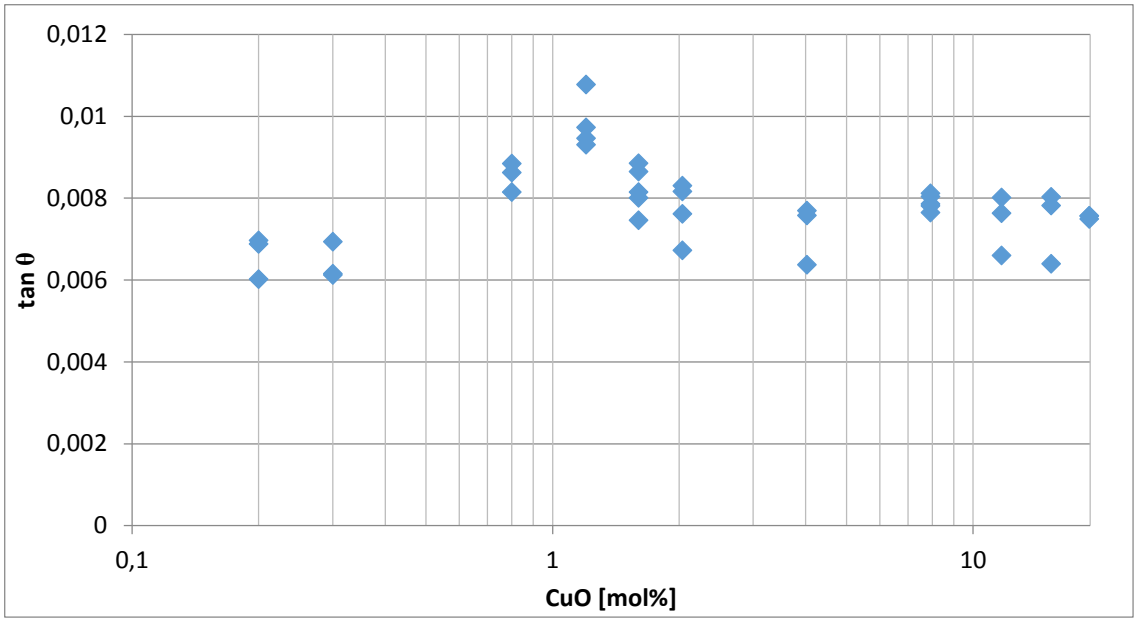

Figure 33 – Loss factor dependent on the copper oxide content at 1 V

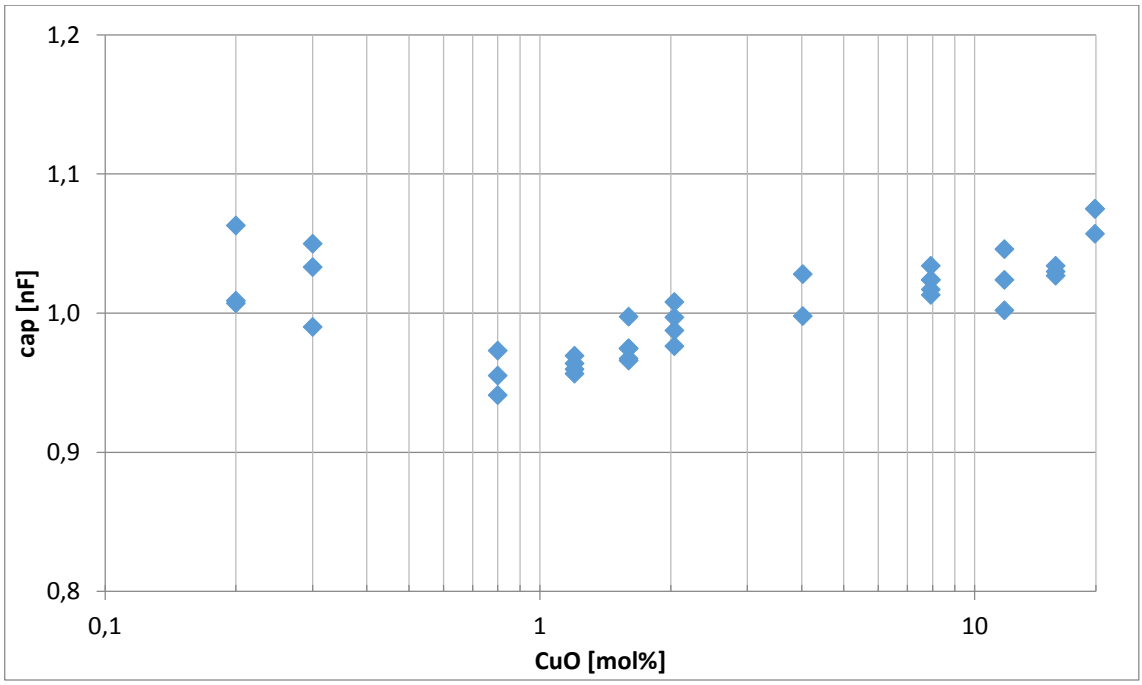

Figure 34 – Capacity in dependency of the copper content of the sample at 1 V

The loss factor (Figure 33) and the capacity (Figure 34) measured at 1 V (small signal) did not show any significant correlation to the copper content.

4 Conclusion

The solubility of copper oxide in PLZT ceramics has its maximum at 0.3 mol%. At this concentration the size of the unit cell stops to grow and decreases slightly with further copper oxide addition. From this increase of unit cell volume it was concluded that Cu^{2+} is incorporated on the B-site of the perovskite lattice up to a concentration of 0.3 mol%. Further these results were confirmed by optical microscopy images, which show colored spots in samples containing at least 0.4 mol% CuO. Those spots, grey in the samples processed in air and red in the samples sintered in reducing atmosphere, were identified as CuO (grey) and Cu_2O (red) by XRD. The assumption about the indication of the limit of solubility by the segregations in the multilayer device was proven. Partly oxidation of the copper electrodes leads to a higher copper content of the material. In the range from 0.3 until 19 mol% copper in disks processed under reducing conditions no significant variation of the electrical characteristics was observed. Disks below 0.3 mol% copper did not sinter properly under the chosen conditions, therefor it was not possible to gain useful results by electrical characterization. Density measurements, optical microscopy and Scanning Electron Microscopy confirmed the function of copper oxide as sintering agent. At 0.4 mol% and at higher copper oxide concentrations a stagnating density was observed. Scanning electron microscopy furthermore confirmed, that there is no influence of the amount of copper oxide on the grain growth.

5 References

[1] **Herbert, J.M.,** High permittivity ceramics sintered in hydrogen, Brit Ceram Trans Journal, 62, 1963, 645-658

[2] **Herbert, J.M.,** Thin ceramic dielectrics combined with nickel electrodes. Proc IEE, 112, 1965, 1474-1477

[3] **Kishi, H., Mizuno, Y., Chazono, H.**, Base metal electrode-multilayer ceramic capacitors: past, present and future perspectives, Japanese Journal of Applied Physics, 1 (42), 2003, 1-15

[4] **Wang, X.X., Murakami, K., Sugiyama, O., Kaneko, S.,** Piezoelectric properties, densification behavior and microstructural evolution of low temperature sintered PZT ceramics with sintering aids Journal of the European Ceramic Society, Volume 21, Issues 10–11, 2001, 1367–1370

[5] https://en.wikipedia.org/wiki/File:Perovskite.svg (23.12.2015)

[6] http://webmineral.com/data/Perovskite.shtml#.Vhz9Cyvh_VI (13.10.2015)

[7] **Goldschmidt, V.M.**, Die Gesetze der Krystallochemie, Die Naturwissenschaften, 21, 1926 477-478

[8] **Eremkin, V.V., Smotrakov, V.G., Fesenko, E.G.** *Fiz. Tverd. Tela*, 31 [6], 1989, 156-161, *Sov. Phys. - Solid State (Engl. Transl.)*, 31 [6], 1989, 1002-1005

[9] **Dheeraj Kumar**, Advanced Physical Chemistry, 2015, 73

[10] **Haertling, G.H., Land, C.E.,** Journal of the American Ceramics Society, 54 [1], 1971, 1-11

[11] **R. D. Shannon** (1976). Revised effective ionic radii and systematic studies of interatomic distances in halides and chalcogenides, Acta Cryst, A32, 1976, 751–767

[12] http://abulafia.mt.ic.ac.uk/shannon/ptable.php (19.10.2015)

[13] **Khomskii D.** Transition Metal Compounds, 2014, 88

[14] **Yoo, J., Chung, K., Lee, D., Jeong, Y.,** Piezoelectric Properties of Low Temperature Sintering $Pb(Co_{1/2}W_{1/2})O_3$-$Pb(Mn_{1/3}Nb_{2/3})O_3$-$Pb(Zr_{0.48}Ti_{0.52})O_3$ Ceramics with the Sintering Temperature and the Amount of CuO Addition, Integrated Ferroelectrics, 69:1, 2006, 159

[15] **Whatmore, R.W., Ringgaard, E.**, Liquid-Phase Sintering of PZT Ceramics, Journal of the European Ceramic Society 20, 2000, 2039-2045

[16] **Nielsen, E.R., Ringgaard, E., Kosec, M.,** Liquid-phase sintering of $Pb(Zr,Ti)O_3$ using $PbO–WO_3$ additive, Journal of the European Ceramic Society 22, 2002 1847–1855

[17] **Prewitt, A.D.** Effects of the poling process on dielectric, piezoelectric and ferroelectric properties of PLZT Dissertation, University of Florida, 2012,

[18] https://de.wikipedia.org/wiki/Blei-Zirkonat-Titanat#/media/File:Hysterese_PZT.png (29.12.15)

[19] **Elaiz-Barranco, A., Hall, D.A.** Influence of Composition and Pressure on the Electric Field-Induced Antiferroelectric to Ferroelectric Phase Transformation in Lanthanum Modified PZT Ceramics, IEEE Transactions on Ultrasonics, Ferroelectrics and frequency control, Vol. 56, No. 9, 2009, 1786

[20] **Martienssen, W., Warlimont, H.** Handbook of Condensed Matter and Materials Data Springer, XVIII, 2005, 1121

6 Appendix

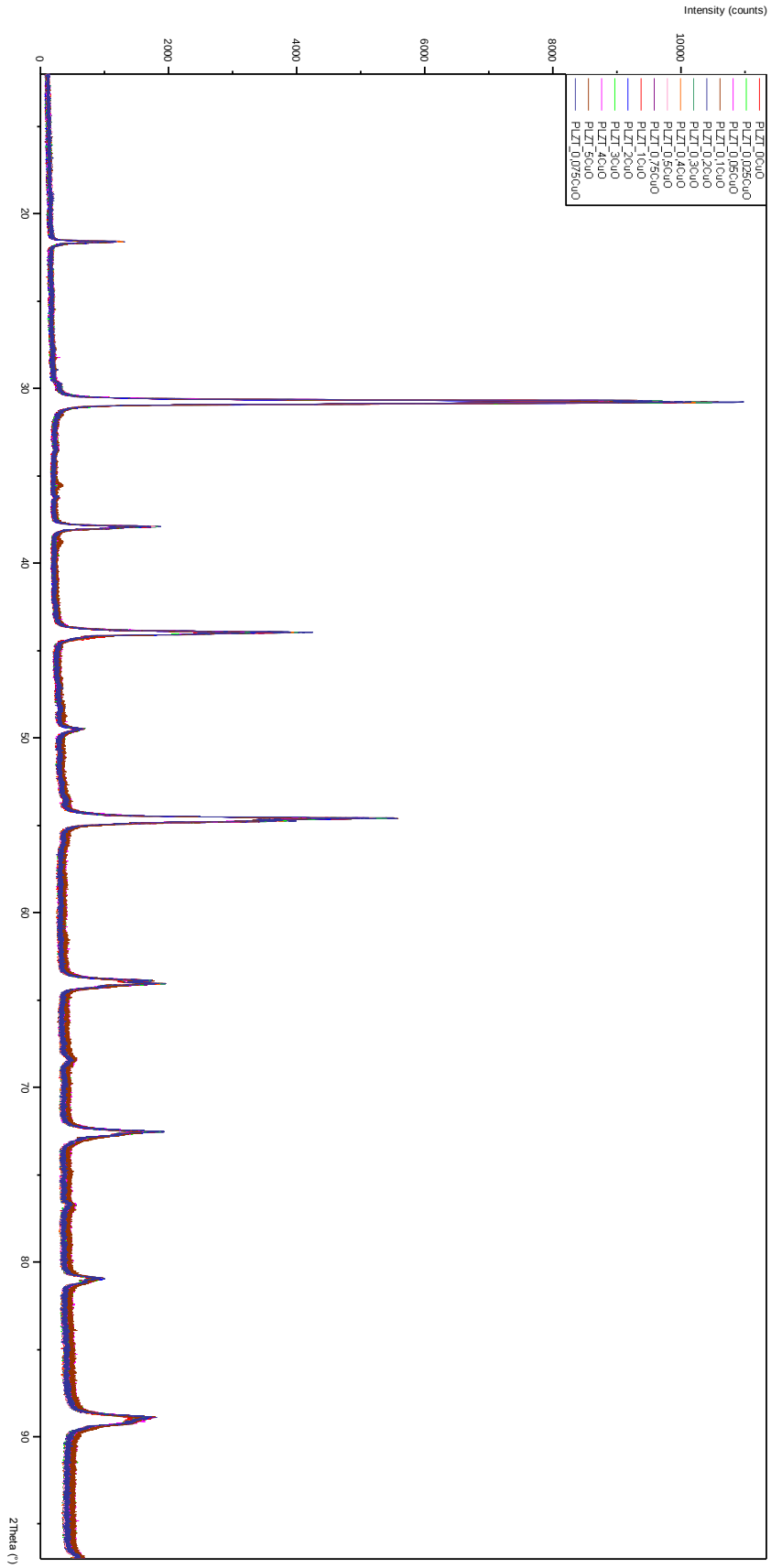

Figure 35 – XRD pattern of the samples processed in air

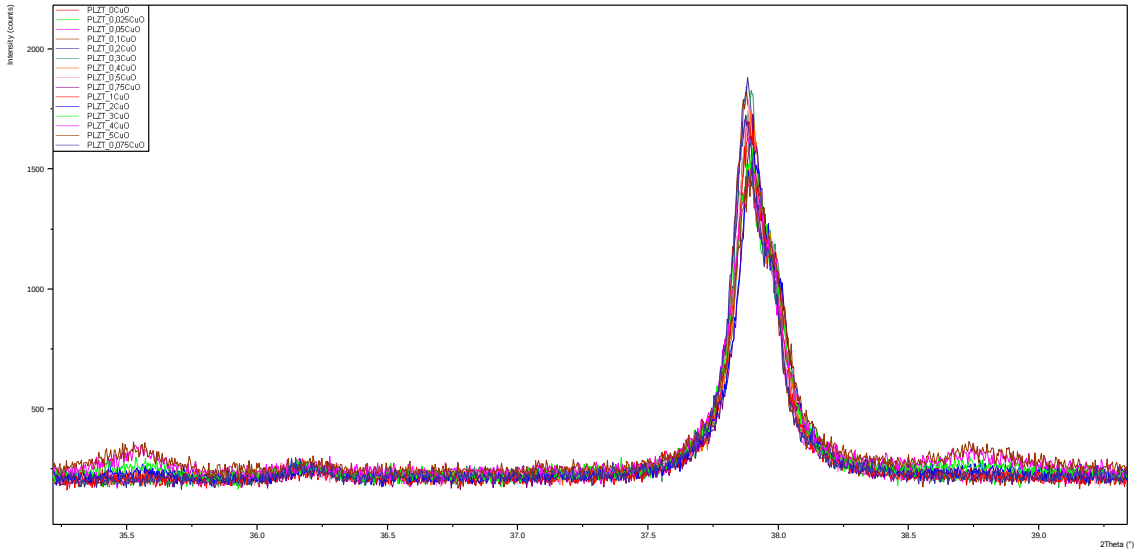

Figure 36 – XRD pattern of the samples processed in air (magnification – with varying copper oxide content CuO peaks are detected 35.5 and 38.75 2Theta)

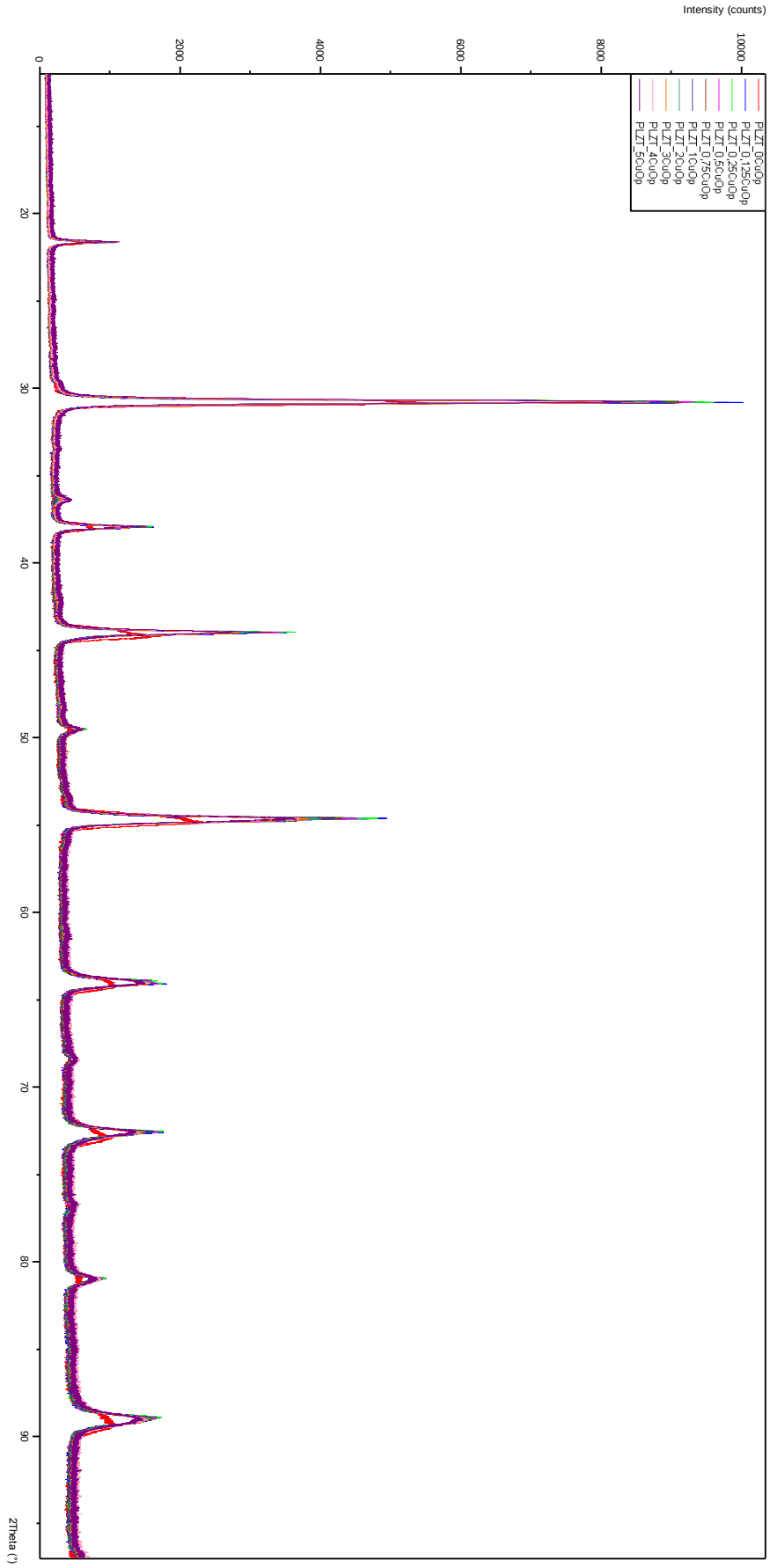

Figure 37 – XRD pattern of samples debindered in air and sintered under reducing conditions

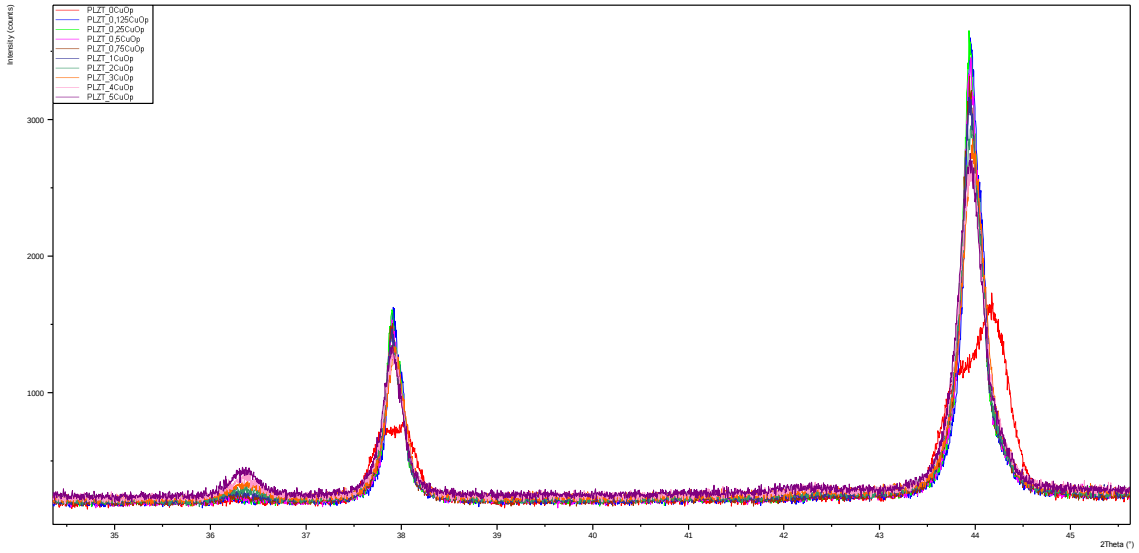

Figure 38 - – XRD Pattern of samples debindered in air and sintered under reducing conditions (magnified to show the influence of the copper content: growth of the copper oxide peak at 36.7 2Theta, sharpening of the perovskite peaks at 38 2Theta and 44 2Theta through function as sintering agent)

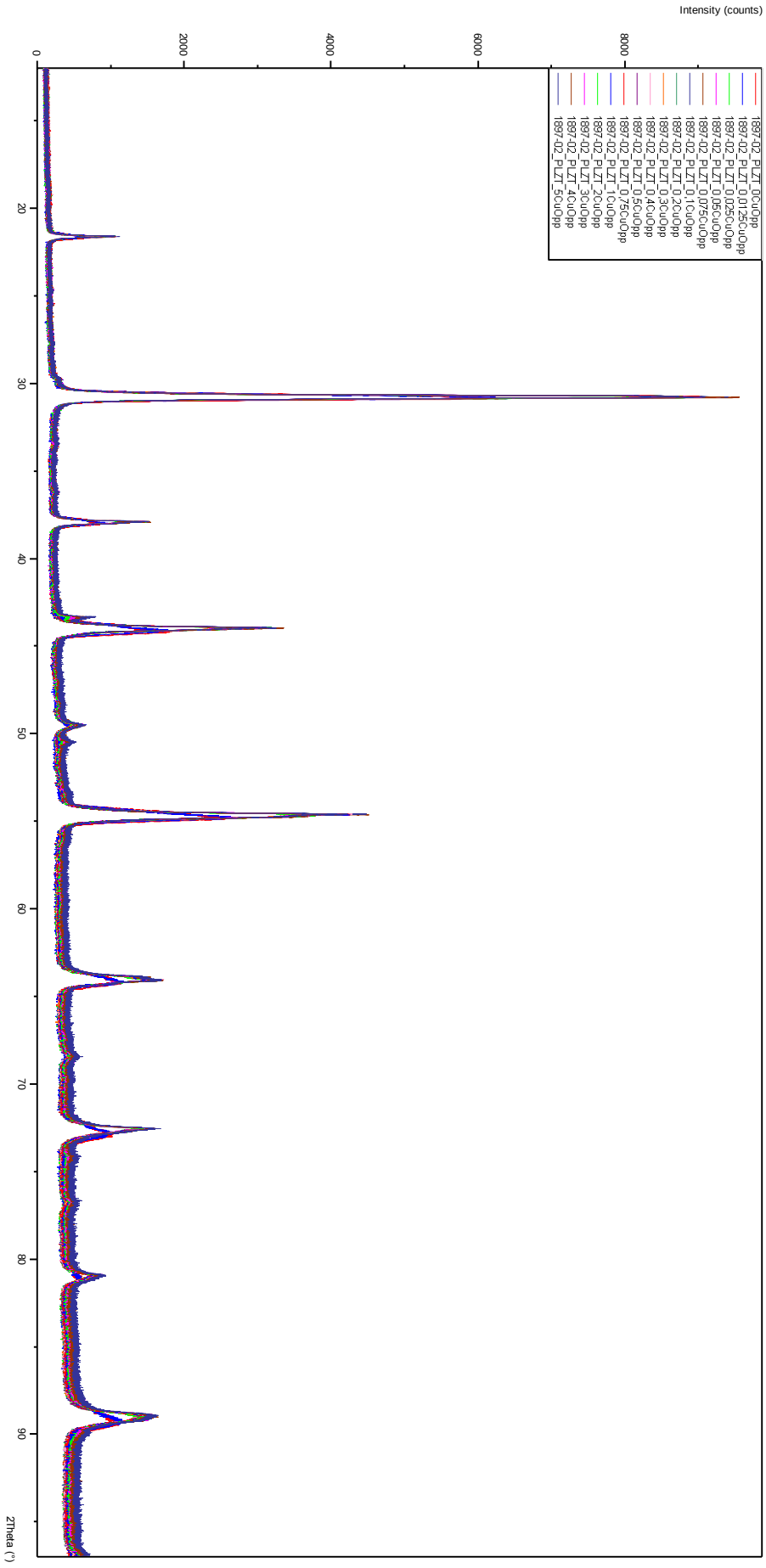

Figure 39 – XRD Pattern of samples debindered and sintered under reducing conditions

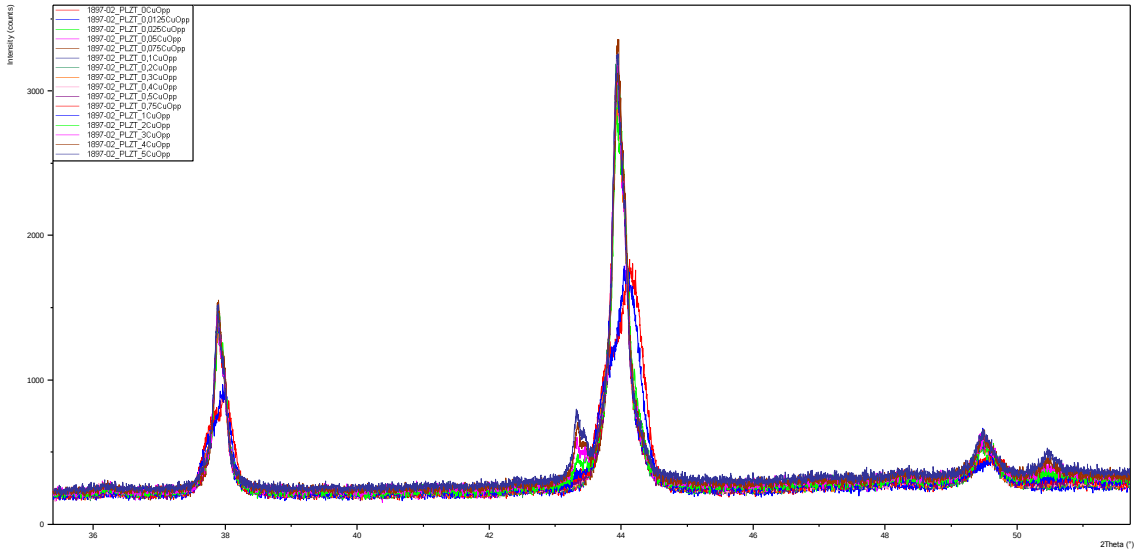

Figure 40 – XRD Pattern of samples debindered and sintered under reducing conditions (magnified to show the interesting region: metal copper 43.5 2Theta and 50.5 2Theta,